FUEL TEMPERATURE INFLUENCE ON THE PERFORMANCE OF A LAST GENERATION COMMON-RAIL DIESEL BALLISTIC INJECTOR.

PART II: 1D MODEL DEVELOPMENT, VALIDATION AND ANALYSIS

Payri, R., Salvador, F.J., Carreres, M. (*), De la Morena, J.

CMT-Motores Térmicos, Universitat Politècnica de València

Camino de Vera s/n, E-46022 Spain.

(*) Corresponding author:

Mr. Marcos Carreres, marcarta@mot.upv.es

CMT-Motores Térmicos, Universitat Politècnica de València

Camino de Vera s/n, E-46022 Spain.

Telephone: +34-963876540

FAX: +34-963877659

Payri, R., Salvador, F.J., Carreres, M., De la Morena, J., "Fuel temperature influence on the performance of a last generation common-rail diesel ballistic injector. Part II: 1D model development, validation and analysis".

Energy Conversion and Management 114 (2016), pp. 376-391 (author version)

ABSTRACT

A one-dimensional model of a solenoid-driven common-rail diesel injector has been developed in order to study the influence of fuel temperature on the injection process. The model has been implemented after a thorough characterization of the injector, both from the dimensional and the hydraulic point of view. In this sense, experimental tools for the determination of the geometry of the injector lines and orifices have been described in the paper, together with the hydraulic setup introduced to characterize the flow behaviour through the calibrated orifices.

An extensive validation of the model has been performed by comparing the modelled mass flow rate against the experimental results introduced in the first part of the paper, which were performed for different engine-like operating conditions involving a wide range of fuel temperatures, injection pressures and energizing times. In that first part of the study, an important influence of the fuel temperature was reported, especially in terms of the dynamic behaviour of the injector, due to its ballistic nature. The results from the model have allowed to explain and further extend the findings of the experimental study by analyzing key features of the injector dynamics, such as the pressure drop established in the control volume due to the control orifices performance or the forces due to viscous friction, also assessing their influence on the needle lift laws.

KEYWORDS

diesel, injection, computational, 1D modelling, fuel temperature

LIST OF NOTATION

A_o orifice outlet area

C_d discharge coefficient

c_f fuel speed of sound

D_{cl} clearance diameter

D_i orifice inlet diameter

D_o orifice outlet diameter

D_{pist} piston diameter

D_{rod} rod diameter

D_{spire} diameter of a spring's single spire

D_{spring} spring diameter

E elastic modulus

F_{pist} piston force

F_{visc} viscous friction force

$F_{\Delta P}$ force due to the pressure difference at both sides of the needle

G shear modulus

K_{eq} equivalent stiffness

K_{spring} spring stiffness rate

$k\text{-}factor$ orifice conicity factor

L length of contact

$\dot{m}$ fuel mass flow rate

$\dot{m}_{th}$ theoretical fuel mass flow rate

N_{spires} number of spires of a spring

P pressure

P_b discharge backpressure

P_{dw} downstream pressure

P_i injection pressure

P_{up} upstream pressure

P_v vapour saturation pressure

p perimeter

Re Reynolds number

T_i fuel injection temperature

t_d delay between SOE and SOI

t_{inj} injection time

u flow velocity

u_{eff} effective velocity

u_{th} theoretical velocity

GREEK SYMBOLS:

ΔP pressure drop

μ_f fuel absolute viscosity

ν_f fuel kinematic viscosity: $\nu_f = \frac{\mu_f}{\rho_f}$

ρ_f fuel density

ABBREVIATIONS:

ET Energizing Time

IRDCI Injection Rate Discharge Curve Indicator

OA Control volume outlet orifice

OZ Control volume inlet orifice

SEM Scanning Electron Microscope

SOE Start of Energizing

SOI Start of Injection

1. INTRODUCTION

The fuel injection system has attracted the interest of researchers in the diesel engine field due to the importance of key aspects such as nozzle geometry, fuel injection pressure or ambient conditions on the air-fuel mixture, combustion efficiency and emissions [1][2][3][4][5][6]. These are key features in the frame of the new standards and regulations in the automotive world, the increasing environmental awareness and the cost of the fossil fuels [7][8]. It is then of crucial importance to understand the diesel injection process in order to propose alternatives that make it possible to optimize its aforementioned outcomes.

In this context, it is helpful to develop computational tools that allow to predict the behaviour of the injection system under several operating conditions, properly catching their influence on the fuel rate of injection and even shaping it as desired [9]. In this sense, one-dimensional modelling seems to be a suitable solution due to its low computational cost as compared to full 3D-CFD approaches, which for this reason are typically focused on specific parts of the injector, such as the nozzle [10][11]. In fact, 1D modelling has already been successfully applied by the authors to study the hydro-dynamic behaviour of the injection system, both in its piezo [12] and solenoid-driven [13][14] variants.

It is important to understand how fuel temperature affects the fuel injection rate, since it is more difficult to control it during the engine operation than it is to control other relevant parameters such as the injection pressure or energizing time. Indeed, fuel temperature strongly affects the fuel properties [15], thus influencing the injected mass flow rate and spray development [16][17], as also noted in the first part of this study. This influence is even more important at extremely low temperatures, representative of cold start conditions [18][19].

Therefore, the computational models need to incorporate the effect of fuel injection temperature to their simulation capabilities in order to increase the accuracy of their predictions. Previous works by the authors regarding fuel injector 1D modelling were restricted to a single fuel temperature [12][13][14]. Different approaches were undertaken by several researchers in order to include fuel injection temperature variations in the simulations. Seykens et al. [20] investigated the effects of the fuel properties on the injection rate by means of a computational 1D model that made it possible to compare the performance of a diesel fuel and a biodiesel fuel at room temperature. Nevertheless, the difference among the properties of these fuels is not representative of the ones that could be induced by differences in temperature when running a diesel engine on its wide range of operating conditions. A similar work by the same authors involved the investigation of a model for a single fuel assuming adiabatic flow inside the injector, but the temperature variations studied were only in the range from 293 to 313 K [21]. Catania et al. [22] emphasized the importance of the effect of the fuel temperature evolution along high-pressure injection systems, also considering temperatures at room conditions or above, as Mohammed et al. [23] also did for the case of hydrogen fuel injection. On the other hand, Plamondon et al. [24] studied the problem for a piezo-driven injector without considering viscous friction, whose effects are deemed to be important on a solenoid injector at low pressure conditions. Different approaches were performed by Rafidah et al. [25], who implemented a 1D model of the whole engine to study the direct effect of the fuel properties on macroscopic variables like fuel consumption, without paying much attention to the injection event itself; or Shi et al. [26], who only focused on the lower part of the nozzle without considering the influence of the control volume orifices performance or the needle movement on the flow, which could also be affected by fuel temperature.

This work aims at the implementation of a 1D model to serve as a tool to predict the performance of a solenoid-driven common-rail ballistic injector (Bosch CRI 2.20), with special attention to the proper modelling of the inlet fuel temperature effects on the injection rate. The model is implemented in the multidisciplinary modelling platform AMESim [27] and validated against data experimentally gathered for a wide range of injector operating conditions (namely injection pressure, energizing time and injection temperature), as described in the first part of the paper. The fuel injection temperature ranges from 253 to 373 K, thus ensuring a proper behaviour of the model within the whole range of engine-like conditions, including cold start. The isothermal approach is considered for the flow, which means that for each simulation the fuel temperature is assumed to be constant along the injector and equal to the one at the injector inlet. Thus, the fuel properties also remain constant within the same simulation. However, the validation highlights that the model is still able to exhibit accurate results while reducing the simulation computational costs, even though the ballistic nature of the injector makes its dynamics more sensitive to the changes in fuel properties (as opposed to previous generations of solenoid-driven injectors studied by the authors [13][14] in which the needle lift was limited to a value - 250 μm - easily achieved during its regular operation, which led to the injector dynamics not being strongly affected by the fuel properties).

Once the model is validated, the simulation results will be used to confirm and explain the findings of the first part of the paper by means of an analysis of the physical processes behind the dynamic behaviour of this kind of injector under extreme temperature conditions. In this respect, the influence of fuel temperature on key features such as the pressure drop established in the control volume, due to the control orifices performance; or the forces on the needle, due to viscous friction, is studied. This allows to link them to the influence on the needle lift laws and the mass flow rate response.

The paper is divided in 6 sections. Section 2 deals with the explanation of the experimental tools used for the injector characterization needed to develop the computational model. This includes both a dimensional and a hydraulic characterization of the injector. Next, Section 3 describes how the different parts of the injector are modelled and implemented into the AMESim software. Section 4 shows the results of the model validation against the experimental results presented in the first part of the paper. Following, in Section 5, the results from the model simulations will be analysed and discussed in order to justify the effect of the fuel temperature on the injection performance. Finally, Section 6 will gather the main conclusions of the study.

2. EXPERIMENTAL TOOLS

The need for a detailed characterization of the injector in order to obtain a reliable model has already been pointed out in Section 1. Both the internal geometry and the hydraulic behaviour of the most important flow restrictions need to be properly implemented in the model. In that regard, efforts must not be spared on obtaining the relevant parameters by experimental means.

The dimensional characterization involves gathering information about the internal lines, orifices, volumes and movable elements of the system, whereas the hydraulic characterization deals with the determination of parameters governing the flow (such as the discharge coefficient behaviour, the detection of cavitation and critical cavitation conditions in such event, etc.) by means of an experimental setup that makes it possible to isolate the flow through one sole restriction at a time. In addition, mass flow rate measurements need to be performed in order to validate the computational model in a wide range of operating conditions.

2.1 Mass flow rate measurements

The main output of the 1D computational model described in this work is the mass flow rate signal. Thus, the validation task needs to ensure that the model responds properly to any change in the injector operating conditions, namely the injection pressure, the fuel temperature and the energizing time. For this reason, mass flow rate results for a wide range of conditions need to be available. The experimental measurements used for validation in the present study were presented in the first part of the paper, covering the conditions summarized in Table 1. These measurements were taken with a commercial IRDCI (Injection Rate Discharge Curve Indicator) placed in a special setup, with particular efforts taken to ensure a proper fuel temperature control. Further details on the IRDCI working principle, setup and signal treatment are given in the first part of the paper, together with the exhibition of the mass flow rate results obtained and used as a basis in the present paper.

2.2 Dimensional characterization

The geometry of the internal ducts and orifices of the injector has been determined by introducing a silicone into the injector body. The silicone methodology to determine nozzle geometries is described by Macián et al. [28], and has been extended to other parts of the injector as shown in Fig. 1. Therefore, silicone moulds of the different parts of the injector are extracted and visualized by either an optical microscope or a SEM (Scanning Electron Microscope), depending on the size of the samples. Thus, the moulds corresponding to larger internal passages can be introduced in the optical microscope. Other large parts of the injector, such as the internal springs, can also be directly visualized in this microscope. Moulds of the small calibrated orifices (such as the inlet orifice – OZ – and the outlet orifice – OA –) and the injector nozzle are visualized in the SEM. Due to the SEM working principle, a gold coating needs to be applied to these samples so that they are able to evacuate the energy of the electron beam. This gold coating is thin enough (in the order of nanometres) not to affect the geometry determination.

Digital pictures of the samples obtained from both the optical microscope and the SEM are processed with a CAD software in order to perform the proper measurements. A summary of the geometrical parameters obtained for the nozzle and the control volume orifices of the injector through this methodology is shown in Table 2. The *k-factor* introduced in the table is defined by Eq. (1) and highlights the high degree of convergence of the OZ and the nozzle orifices, whereas the OA orifice is essentially cylindrical. This means that the former orifices are not prone to cavitate, as opposed to the latter [29]. This finding is confirmed by the hydraulic characterization (Section 2.3) and taken into account on the modelling.

$$k - factor = \frac{D_i - D_o}{10} \qquad (1)$$

2.3 Hydraulic characterization

The main purpose of the hydraulic characterization of an orifice is to determine its flow behaviour depending on the operating conditions of the injector. This characterization can be performed by analysing the continuous flow through the orifice under several conditions of upstream and downstream pressure. To this end, the experimental setup depicted in Fig. 2 has been used. An electrically-driven fuel pump extracts the fuel from a tank and pressurizes it after going through a filter, providing continuous flow. Since the fuel heats up due to its pressurization, a fuel-water heat exchanger is used to cool down the flow before reaching a commercial common-rail, where the pressure is controlled thanks to a manual regulation valve located upstream of the rail. The hydraulic restriction to be characterized (either the nozzle or a control volume orifice) is disposed downstream of the rail, inside a test rig that isolates the corresponding orifice, avoiding any leakage to other paths. Details on the test rigs for the nozzle and the control volume are given in Sections 2.3.1 and 2.3.2. Fuel flows through the hydraulic restriction into a discharge chamber, where the backpressure is controlled by means of another manual regulation valve located downstream of the chamber, and is finally injected into a glass deposit where the fuel mass instantaneously injected can be measured thanks to a scale. After a short stabilization time for each measurement, the mass flow rate is determined by averaging it for a period of 100 seconds.

2.3.1 Nozzle test rig

Fig. 3 shows the test rig for the hydraulic characterization of the nozzle, which ensures proper sealing. The nozzle is introduced without the needle, so that only the flow features through the orifices themselves are accounted for.

As stated in the first part of the paper, the mass flow through an orifice is given by the mass conservation equation, in which the discharge coefficient is introduced to take the losses into account:

$$\dot{m} = \rho_f \, A_0 \, u_{th} \, C_d \qquad (2)$$

with u_{th} being the theoretical velocity through the orifice, derived from Bernoulli's equation taking the assumption of negligible upstream velocity, as described by Eq. (3):

$$u_{th} = \sqrt{\frac{2\Delta P}{\rho_f}} \tag{3}$$

where $\Delta P = P_{up} - P_{dw}$. The discharge coefficient can then be obtained as:

$$C_d = \frac{\dot{m}}{A_0\sqrt{2\rho_f\left(P_{up} - P_{dw}\right)}} \tag{4}$$

The discharge coefficient strongly depends on the theoretical Reynolds number, defined as:

$$Re = \frac{\rho_f\, u_{th}\, D_0}{\mu_f} \tag{5}$$

In order to ensure a wide range of Reynolds numbers, two values of upstream pressure (10 and 20 MPa) are tested, whereas a sweep of downstream pressures from atmospheric pressure to 8 MPa (mechanical limit of the test rig) is carried out for each upstream pressure.

Results from the nozzle hydraulic characterization are depicted in Fig. 4. The left side of the figure shows the mass flow rate against the square root of the pressure drop. A linear trend is observed for both values of upstream pressure, as expected [4]. The fact that a mass flow rate collapse is not seen points out that the nozzle orifices do not work under cavitating conditions, confirming what was stated in Section 2.2 as suggested by their high *k-factor* [29]. With regard to the behaviour of the discharge coefficient with respect to the Reynolds number, shown at the right side of the figure, the asymptotic trend expected from the literature [30] can also be guessed by the experimental results. The discharge coefficient tends to a maximum value of about 0.96. This value is important for the model since AMESim takes it as a reference and uses the so-called critical Reynolds number Re_{crit} (Reynolds number at which the discharge coefficient is 95% of the maximum value) as the transition between laminar and turbulent flow, implementing the following C_d vs Re law [27]:

$$C_d = C_{d_{max}} \tanh\left(\frac{2Re}{Re_{crit}}\right) \qquad (6)$$

In the case of the nozzle orifices, Re_{crit} takes a value of 5600. The evolution of C_d with Re predicted by AMESim according to Eq. (6) and the parameters that have been found through the hydraulic characterization are also shown in Fig. 4, revealing a proper fit to the experimental points.

2.3.2 Control volume orifices test rig

The test rig for the hydraulic characterization of the control volume orifices is shown in Fig. 5 together with the injector control volume itself. There are two different configurations in which the test rig can be mounted in the experimental setup described in Fig. 2. In order to characterize the OA orifice, the port at the left side of the test rig in the figure is locked, and the test rig is mounted on the experimental setup so that the fuel flows from the bottom of the control volume to the top. The same test rig can be used for the OZ orifice characterization by locking the upper port of the test rig and making the fuel flow from the OZ orifice entrance to the lower part of the test rig.

Fig. 6 shows the results of the OA orifice hydraulic characterization. As it was done for the nozzle orifices, the left side of the figure shows the mass flow through the orifice against the square root of the pressure drop. A linear trend is also observed until a mass flow rate collapse is noticed for each upstream pressure, indicating cavitation inside the orifice, as expected due to its cylindrical shape reported in Section 2.2. The conditions at which the mass flow starts being choked are the critical cavitation conditions and also need to be provided to the AMESim model. Since cavitation is observed for all the tested values of downstream pressure (from atmospheric pressure to 8 MPa, as tested for the nozzle orifices) for the upstream pressure of 20 MPa, an intermediate level of upstream pressure (15 MPa) has also been tested, so that the critical cavitation conditions determination is more reliable. The right side of the figure shows the behaviour of the discharge coefficient against the Reynolds number. It can be seen that, when the orifice works under non-cavitating conditions, the same trend that was analysed for the nozzle orifices is observed. However, for each upstream pressure, the discharge coefficient drops abruptly once the orifice starts cavitating. This fact highlights the need to properly describe the transition from non-cavitating to cavitating conditions in order to predict the injector behaviour in an accurate way.

The proneness of an orifice to cavitate has been described in the literature through different approaches. The cavitation number, *CN*, introduced by Soteriou et al. [31] is used in the present work:

$$CN = \frac{P_{up} - P_{dw}}{P_{dw} - P_v} \qquad (7)$$

where P_v is the saturation vapour pressure of the fuel. This term is usually neglected due to its low value when compared to the others, thus leading to:

$$CN = \frac{P_{up}}{P_{dw}} - 1 \qquad (8)$$

For each value of upstream pressure, the critical cavitation number CN_{crit} is defined as the cavitation number for the downstream pressure that leads to cavitation conditions, which can be determined from Fig. 6. The behaviour of the discharge coefficient in non-cavitating conditions, where it depends on the Reynolds number, has already been discussed. However, in cavitating conditions, its behaviour can be described as a function of the cavitation number, as reported in the literature [31][32] and stated in Eq. (9):

$$C_d = C_c \sqrt{1 + \frac{1}{CN}} \quad (9)$$

where C_c is the contraction coefficient, which describes the loss in discharge coefficient associated to the lower effective area in an orifice due to the presence of vapour bubbles. C_c can be obtained by applying Eq. (9) for the particular case of the critical cavitation conditions, for which both C_d and CN are known.

A summary of the relevant parameters obtained from the hydraulic characterization of both the nozzle orifices and the control volume orifices (OA and OZ) is given in Table 3. It is important to note that cavitation has not been noticed for the OZ orifice, as expected due to its high *k-factor* reported in Section 2.2.

3. INJECTOR MODELLING

As stated before, AMESim has been used as the platform to implement the injector model [27]. It is a commercial simulation software for one-dimensional modelling and analysis. This software consists of a set of components from predefined libraries that belong to the different physical domains. Thus, the assembly of components makes it possible to simulate and analyse multi-domain systems. In the case of the injector, libraries from the electrics, mechanics and hydraulics fields are used, among others. For illustrative purposes, the model implemented in this work is divided in three parts that are described in the present Section: the injector holder, the solenoid valve and the nozzle. The implementation of the fuel properties is also described here.

3.1 Injector holder

Fig. 7 shows a sketch of the injector holder together with its model representation. A pressure source element is used in order to simulate the high pressure pump, which raises the pressure in a volume that represents the common-rail upstream of the injector inlet. Right at the injector inlet, the flow travels through the high pressure filter, modelled as a flow restriction. From here, the flow passes through the line HL1 until it reaches a bifurcation: part of the fuel enters the injector control volume HV1 through the OZ orifice. The pressure on this volume is used to compute the pressure force on the upper part of the needle, mechanically modelled as the element P1. The flow is also allowed to leave the control volume through the HL2 line linked to the OA orifice, connected in turn to the HV2 volume that links the injector holder to the solenoid valve. The rest of the fuel after the bifurcation downstream of the HL1 line travels to the nozzle through lines HL3, HL4 and HL5 in order to be injected into the cylinder. This fuel also encounters the volumes HV3 and HV4, where the pressure forces on other parts of the needle are computed.

It is important to note that the main parameters of the hydraulic lines are their length and diameter. For those cases in which the hydraulic line is not circular (such as lines HL4 and HL5, which are annular ducts), the hydraulic diameter defined in Eq. (10) is used instead:

$$D_{hydr} = \frac{4 \cdot A}{p} \qquad (10)$$

where A is the cross-sectional area of the duct and p the associated perimeter.

As far as the mechanical elements of the injector holder are concerned, the upper part of the needle is modelled by the elements P1, NLF, P2, 1/2 NM, ND and NSP. The piston P2 computes the pressure forces due to a change in area in the needle that generates an annular surface on which the pressure in the HV3 volume acts, trying to push the needle upwards. Any piston element computes the pressure forces from the pressure P in its associated volume as:

$$F_{pist} = \frac{\pi}{4} P\left(D_{pist}^2 - D_{rod}^2\right) \tag{11}$$

The element 1/2 NM accounts for half of the needle mass, since the other half will be linked to the nozzle part due to compatibility among AMESim elements. Friction in the mass elements is taken into account through a static friction term that needs to be overcome prior to the mass movement, and a viscous friction term that is a direct function of the fluid viscosity. Moreover, the NLF element accounts for internal leakages and viscous friction that take place due to the small clearance among the needle and the injector holder itself in certain parts of the injector. Flow through this clearance is considered with the Poiseuille law, assuming laminar regime. The viscous friction is then computed as stated by Blackburn et al. [33]:

$$F_{fric} = -\Delta P \cdot \pi \cdot \frac{D_{cl} \cdot \left(D_{pist} - D_{cl}\right)}{4} + 4 \cdot \pi \cdot \mu_f \cdot u \cdot L \cdot \left(\frac{D_{pist}}{D_{cl}} - 1\right) \tag{12}$$

where D_{cl} is the clearance diameter among the needle and the injector holder, u is the mean flow velocity, L is the length of contact along which the needle and the injector holder are only separated by a small gap and ΔP is the pressure difference across the element. In the case of the needle, this pressure difference is the one set among the volumes HV1 (control volume) and HV3. During the normal operation of the injector, the pressure in the control volume will depend on the pressure drop across the OZ orifice, whereas the pressure in the HV3 volume is approximately the rail pressure, since no important flow restrictions are found in the high pressure filter or the HL1 and HL3 lines. Thus, the pressure drop in the control volume and the fuel viscosity are key on understanding the friction forces on the needle.

In addition, NSP represents the spring that tries to hold the needle against its seat and opposes to its lift. The stiffness rate of all the springs in the model has been calculated from their geometry through the equation established by Adler and Bauer [34]:

$$K_{spring} = \frac{G \cdot D_{spire}^4}{8 \cdot N_{spires} \cdot D_{spring}^3} \qquad (13)$$

where G is the shear modulus of the material (steel), D_{spire} is the diameter of a single spire of the spring, i.e. its thickness, D_{spring} is the diameter of the whole spring and N_{spires} is the spring total number of spires.

Finally, the element ND represents the elastic deformation of the needle, especially relevant prior to the injection event, when the needle is closed against its seat and the high pressures of the system lead to deformations that need to be recovered before the needle effectively opens once the injector is energized. These deformations are computed through an equivalent spring whose stiffness rate is calculated by means of the equation established by Desantes et al. [35]:

$$K_{eq} = \frac{1}{\frac{1}{E}\sum\frac{L_i}{A_i}} \qquad (14)$$

where E is the elastic modulus of the material, whereas L_i and A_i are the length and cross section of each segment of the needle with the same cross-sectional area, respectively.

A summary of the most important parameters introduced in this part of the model is presented in Table 4. These parameters were gathered as described in Section 2.2. Details on the control volume orifices were presented in Section 2 and thus are here omitted.

3.2 Solenoid valve

A detail of the solenoid valve part of the injector together with a zoom to the magnetic path and the corresponding AMESim sketch proposed are shown in Fig. 8. The mechanical elements (piston) of the valve are in charge of avoiding any flow from the control volume (HV1) through the OA orifice when the injector is not energized. When current arrives to the solenoid coil, it induces a magnetic flux through the magnetic core (represented by the elements SM1, SM2 and SM3) that crosses the air gap AG towards the upper side of the valve piston (SM4). This magnetic flux depends on the material, length and area of the elements it trespasses, which are obtained thanks to the injector dimensional characterization. The main parameters of the magnetic part of the solenoid valve are summarized in Table 5. The magnetic coil resistance has been determined by means of a commercial digital multimeter.

The resulting magnetic flux is responsible for the generation of a force that attracts the valve piston, letting the fuel flow from the control volume through an orifice, whose cross-sectional area grows as the valve piston moves up. Hence, this orifice has been modelled as the SO1 restriction, whose hydraulic diameter is a function of the valve piston lift (which is limited to 20 μm) and is linked to the injector holder part of the model through the OA orifice. Therefore, when the injector is energized, the set consisting of the OA and SO1 orifices evacuates fuel from the control volume, thus dropping its pressure and letting the needle rise, producing the injection. The fuel leaving the control volume flows to the return line through the SO2 orifices carved at both sides of the upper part of the control volume piece. From there, it travels through the SO3 orifices, drilled on the valve piston, and leaves the injector through the lines SL1 and SL2 and the orifice SO4, which represent the return duct. Along this path, the fuel also encounters the volumes SV1, SV2 and SV3, whose pressure acts on the pistons SP1, SP2, SP3 and SP4 that generate the forces that help opening or closing it against the SO1 orifice, in an analogous way to the piston forces on the needle explained in Section 3.1. These pistons, together with the valve mass VM, shape the valve piston mechanical part. A displacement sensor VDS is also introduced in the model to transfer the valve piston lift to the SO1 orifice at all times, establishing its variable area. In addition, the SLF element accounts for the internal leakages and viscous friction in this section of the injector, in a similar way to the one described for the needle in Section 3.1.

Once the injector stops being energized, the valve piston closes the SO1 orifice thanks to the force imposed by the SS spring. In this situation, the OZ orifice refills the control volume, restoring its pressure and making the needle close against the nozzle seat, cutting the injection.

A summary on the most important parameters of the solenoid mechanical part is shown in Table 6.

3.3 Nozzle

Fig. 9 shows the nozzle together with its AMESim equivalent sketch. The fuel comes from the injector holder part through three parallel lines NL1 resulting from the quasi-triangular needle cross-section. For each of the lines, an additional hydraulic orifice NO1 has been introduced due to an increase in the needle cross-section, which results in an important restriction to the flow that may lead to important pressure changes. After these orifices, the fuel keeps travelling along parallel ducts NL2, until they encounter each other in the NV1 volume, from where it flows to the nozzle orifices through the nozzle channel NL3. The volume at the lower part of the nozzle is divided into the NV2 and NV3 volumes, since the latter exclusively represents the sac, considered from the needle seat point onwards. The NV1 and NV2 volumes are associated to the pistons NP1 and NP2 that will simulate the pressure forces pulling the needle upwards. The nozzle seat NST is represented by a conical seat element that accounts for both the needle tip and the seat, and thus computes an additional pressure force associated to the sac (NV3 volume). The rest of the needle mass NM is associated to this part of the model. When the needle lifts, it discovers the 7 orifices of the nozzle, leading to the fuel being injected to a tank at a given backpressure.

The determination of the parameters associated to the nozzle seat NST is especially critical. Thanks to the dimensional characterization technique explained in Section 2.2, it is possible to obtain them by overlapping optical microscope pictures of both the needle and the nozzle silicone mould, as shown in Fig. 10.

The main parameters introduced into the nozzle part of the model are shown in Table 7. Details on the geometry of the nozzle orifices were already given in Section 2.2 and summarized in Table 2.

3.4 Fuel properties

As stated in the first part of the paper, the fuel used for the mass flow rate measurements that comprise the basis for the validation of the computational model proposed in this work is a standard winter fuel. Its properties were determined for a wide range of temperatures at atmospheric pressure and are available for the model. It was already stated in the Introduction section that the model will introduce the hypothesis of isothermal flow, thus keeping the temperature at the inlet as a constant along the injector, without changes in the fuel properties within the same simulation. Table 8 reminds the values of density and absolute viscosity that were used for the temperatures for which the model has been validated.

4. MODEL VALIDATION

In order to ensure a proper behaviour of the model at the wide conditions of engine operation, the model has been validated against the experimental results of mass flow rate obtained in the first part of the paper, whose conditions are summarized in Table 1.

Fig. 11 shows a comparison of the mass flow rate curves obtained from the model versus the experimental ones at different injection pressures for each injection temperature. Three curves corresponding to different ET (0.5, 1 and 2 ms) are depicted for each P_i and T_i. It can be seen that the model properly reproduces the injector behaviour for most of the tested conditions. The stationary mass flow rate follows the observed trends with the injection pressure and temperature, with a small underprediction for the highest temperature tested. With regard to the injection duration, the trends are also preserved except for the prediction of shorter durations for the energizing times of 0.5 ms for the temperatures of 303 K and higher. The analysis of the opening slope reveals a good reproduction of reality by the model, which appropriately follows the observed trend with the injection temperature. The worst results are obtained for the lowest injection temperature, for which the model assumes a slower opening slope. This fact can be attributed to the assumption of isothermal flow, which is not totally representative of the injector internal flow due to the heating that may take place especially through the small calibrated orifices (i.e. control volume and nozzle orifices), where viscous friction effects are deemed to be important. Thus, the isothermal assumption works properly for temperatures over 273 K due to the small changes in the relevant fuel properties (i.e. density and viscosity) associated to fuel heating in that case, whereas the behaviour is slightly worse for the cold temperature range, for which the viscosity follows an exponential trend (Table 8).

Since it is also important for engine modellers to be able to accurately predict the total mass injected into the cylinder, the reliability of the model is assessed in these terms in Fig. 12, where the values of total mass injected obtained from the model are compared against the experimental ones. Results show a fair prediction for the majority of points studied. More than 80% of the points are within a deviation lower than 10%. The highest deviations are noticed at low injection temperatures, representing up to 7% in the case of long injections (energizing times of 1 ms and 2 ms) or 35% in the case of the short injections (energizing times of 0.25 and 0.5 ms), where small deviations in absolute terms lead to a high percentage of deviation even if the injection rate shape is properly predicted. On the contrary, for the highest injection temperature, differences are lower than 10% for all the tested points. These findings are a direct consequence of the differences in mass flow rate curves observed in Fig. 11.

5. RESULTS AND DISCUSSION

Fuel temperature is expected to influence the flow along the injector, especially through the most important restrictions (nozzle and control volume orifices), due to the different density and viscosity values induced. The density affects the mass flow rate through the restriction, in addition to controlling the flow regime together with the viscosity through the Reynolds number. These facts were already analyzed in the first part of the paper from the point of view of the stationary mass flow rate at the injector outlet. However, they are also deemed to play a key role on injector dynamics. In this case, a deeper analysis of the internal flow is required in order to explain the differences associated to the fuel temperature. The present Section aims at the internal exploration of the injector by means of the implemented computational model, further analyzing the simulations corresponding to the operating conditions used for validation, in order to identify and assess the causes for the differences related to fuel temperature.

Fig. 13 shows a simplified sketch of the injector depicting the main phenomena involved during the transient stages of the injection. On the one hand, injector dynamics are influenced by the force due to the pressure difference between the upper part of the needle (control volume) and its lower part. This pressure difference is governed by the performance of the control volume orifices, since the flow rate through them determines both the ability to evacuate the control volume when the solenoid valve is energized (thus reducing the pressure at the upper part of the needle, making it rise discovering the nozzle orifices) or to refill it when the injector stops being energized (recovering the pressure at the upper part of the needle and making it close against its seat). These features can be studied through the internal analysis of the injector allowed by the computational model. On the other hand, needle dynamics are influenced by the force generated by viscous friction in the clearance between the needle and the injector wall, especially when this clearance is small. This viscous friction depends on the fuel viscosity, as stated by Eq. (12), which in turn depends on the fuel temperature. The fact that this friction force also depends on the pressure difference established between the control volume and the rail (as justified in Eq. (12)) makes it difficult to isolate the effects of the fuel temperature exclusively related to the control volume orifices performance from those related to the change in fuel properties. However, they will be hereby analyzed and linked to the needle lift evolution during the injection event, which should explain the findings from the experimental mass flow rate measurements.

5.1. Analysis of the hydraulic parameters of the flow through the control volume orifices

As it has been mentioned, the hydraulic parameters of the control volume orifices play a key role on injector dynamics, since they determine the ability to effectively fill or empty the control volume, generating the pressure difference that drives the needle. During the opening stage, the OA orifice is uncovered and becomes responsible for evacuating the fuel from the control volume, whereas the losses through the OZ orifice, which is always active, determine the pressure drop in the control volume. During the closing stage, the OA orifice is locked and the discharge capabilities of the OZ orifice determine the ability of the control volume to recover its pressure. Attention to the discharge coefficients of both orifices must be given in order to shed light on these phenomena, keeping in mind that the OZ orifice is not expected to cavitate for any of the engine operating conditions due to its high conicity (recall Section 2), whereas the OA orifice is prone to cavitate.

Fig. 14 shows the simulated discharge coefficients of the control volume orifices as a function of *Re* (OZ orifice and non-cavitating region of the OA orifice) and the *CN* (cavitating zone of the OA orifice), representing where the tested conditions are located. In the case of the OA orifice, it can be seen that the orifice is cavitating ($CN > CN_{crit}$) for all the tested conditions, but the non-cavitating part of the curve has been respected for illustrative purposes. No influence of the fuel temperature on the discharge coefficient has been found for temperatures higher than 303 K. In the case of the OZ orifice, Re is above Re_{crit} for all these conditions, directly leading to C_{dmax}. For the OA orifice, the pressure drop across the orifice remains the same regardless the nominal injection pressure, since the flow will experience subsequent pressure drops downstream the orifice due to the presence of further restrictions (SO1) before reaching the atmospheric pressure at the return line. An influence of the fuel temperature is however noticed at low temperatures. In the case of the OZ orifice, the high fuel viscosities associated to the low fuel temperatures (recall Table 8) lead to changes in the flow regime for the T_i = 253 K and T_i = 273 K cases, making the orifice work under the laminar regime in the former, whereas it acts on the laminar-turbulent transition on the latter. This results in a drastic reduction of the flow discharge capabilities across the OZ orifice, which is expected to lead to low pressures in the control volume during the opening. In the case of the OA orifice, the fuel temperature has only been found to affect CN for the lowest temperature tested, in a more important manner for the lower injection pressures. However, the associated differences in discharge coefficient are less significant.

Fig. 15 shows the evolution of the pressure at the control volume for the whole range of temperatures studied and two different injection pressures, focusing on the cases of ET = 1 ms. The pressure values have been normalized with respect to the nominal injection pressure. Results for T_i = 353 K have been omitted due to their similarity with the ones at T_i = 373 K. The figure shows that the depression generated at the control volume at the opening stage is more important the lower the fuel temperature. This result can be explained due to the differences in mass flow rate expected at both control orifices. On the one hand, these differences come from the fact that the fuel density decreases linearly when increasing the fuel temperature (recall Table 8). However, Fig. 15 shows that the differences in the pressure drop at the control volume at different temperatures become more important at the lowest temperatures, which suggests a non-linear trend. This is consistent with the findings about the discharge coefficients shown at Fig. 14, where the changes in flow regime induced by the lowest temperatures lead to further limitations on the OZ orifice discharge capabilities, producing extra losses on the orifice and therefore lower pressures set downstream. The performance of the OA orifice was already demonstrated to be only slightly affected by fuel temperature in the most extreme cases. Another factor that cannot be neglected when analyzing the pressure changes in the control volume is the fact that the needle lift evolution is expected to be different depending on the fuel temperature, thus modifying the actual size of the control volume, which therefore will lose or recover pressure at a different rate. No significant differences are appreciated among injection pressures, although it can be seen that a lower relative pressure drop is achieved for the highest injection pressure. This can be explained due to the fact that a higher mass flow rate enters the control volume through the OZ orifice, hindering the process to evacuate it.

It is important to note that the sole effect of the discussed control volume orifices hydraulic parameters would lead to a faster response of the injector at low temperatures, due to the more accused pressure drop at the control volume, which generates a higher unbalance at both sides of the needle. However, as stated before and highlighted by Fig. 13, the effect of the friction force also needs to be analyzed.

5.2. Analysis of the friction force opposing the needle movement

As shown by Eq. (12), the friction forces appearing on the needle when trying to lift through the fuel depend both on the pressure drop along the needle and the fuel viscosity, with opposed effects. Fig. 16 shows the evolution of the needle friction force for all the range of temperatures studied and P_i = 70 MPa (results for P_i = 180 MPa have been omitted since the trend has been found to be the same), focusing on the cases of ET = 1 ms. Values have been normalized with respect to the case of T_i = 303 K, representative of ambient temperature. The figure only shows the time range corresponding to the stage in which the needle is rising. It can be seen that the friction forces are extremely affected by fuel temperature, getting higher the lower the temperature. Analyzing the two terms of Eq. (12), the higher pressure drops in the control volume observed at low temperatures (recall Fig. 15) would act in the sense of reducing the friction force. However, the increase in fuel viscosity at low temperatures acts with an opposite sense. The exponential trend of the fuel viscosity at low temperatures (recall Table 8) is able to overcome the effect of the pressure drop and justifies the higher friction forces observed in those cases. Thus, it is possible to state that the net effect of increasing the fuel temperature is a reduction in the friction force, which would in turn act in the sense of a faster needle opening.

5.3 Analysis of the combined effect of control volume pressure drop and friction forces on needle dynamics

As highlighted by Fig. 13, injector dynamics are influenced, on the one hand, by the force due to the pressure difference between the control volume and the nozzle sac, being affected by the friction force on the other side. As it has been demonstrated in Sections 5.1 and 5.2, a lower fuel temperature would lead to a faster injector opening if only the pressure forces were considered, whereas it would lead to a slower opening by the sole effect of viscous friction. The present subsection aims at the analysis of the net effect of both phenomena in order to understand how the fuel temperature influences needle dynamics.

Fig. 17 shows the needle lift evolution obtained from the simulations for the whole range of temperatures studied and two different injection pressures, focusing on the cases of ET = 1 ms. Needle lift values have been normalized with respect to the injector's mechanical limit (850 µm).

The figure shows that the time at which the injector closes depends on the fuel injection temperature, as concluded in the first part of the paper due to the ballistic nature of the injector. It is observed that the needle opening is slower the lower the fuel temperature. In order to explain the net effect of the fuel temperature on the opening stage, Table 9 summarizes the effects of the fuel temperature on the control volume pressure and the friction force for the case of P_i = 70 MPa at a time after SOE of 0.7 ms. Values have been extracted from Fig. 15 and Fig. 16 and normalized taking the case of T_i = 303 K (representative of ambient conditions) as a reference. It can be seen that, in the end, the effect of the fuel temperature on the friction force is more important than the one on the control volume pressure through the differences in flow through the control volume orifices. Thus, the opening stage of the injection event is governed by the friction force appearing on the needle due to viscous effects, resulting in a slower opening the lower the fuel temperature is.

Fig. 17 shows that a slower needle opening results in lower top positions reached by the needle during an injection event. Hence, during the closing stage, the needle falls from these lower positions for low injection temperatures, which results in shorter times needed for the needle to close against its seat and cut the injection.

Fig. 18 summarizes the highest position reached by the needle for all the tested operating conditions. The expected trends in the view of Fig. 17 are followed except for high injection pressures ($P_i \geq$ 120 MPa) and long energizing times (ET > 1 ms), where the needle already reaches its mechanical limit. This explains the fact that, at the longest energizing times (2 ms), the injection duration does not always follow the same trend with the injection pressure, as had already been noticed in the first part of the paper through the experimental measurements, and can be observed in Fig. 11: in general, for a given energizing time, the injection duration is longer the higher the injection pressure, due to the higher maximum positions of needle lift reached due to the pressure forces. This is no longer true when there are several injection pressures for which the limit needle lift is achieved, since in those cases the needle falls from the same position and the only effect on injection duration is the one due to the needle closing speed, related to the previously mentioned phenomena.

6. CONCLUSIONS

The fuel temperature influence on injector dynamics has been assessed in this paper through a computational 1D model of a last-generation common-rail diesel ballistic injector implemented in the AMESim platform. The methodology to develop such a model through a careful characterization (both dimensional and hydraulic) has been presented, and its validity has been demonstrated in a wide range of fuel temperature conditions, from 253 to 373 K, obtaining a reasonable reproduction of the mass flow rate curves. Results have been analyzed through simulations at those temperature conditions and different levels of injection pressure and energizing time.

The main conclusions of the study are summarized in the following points:

- Injector dynamics are mainly affected by the pressure difference established between the control volume and the nozzle sac on the one hand, and the friction force generated between the needle and the fuel due to viscous effects on the other hand.

- The pressure established at any time in the control volume depends on the performance of the control volume orifices (OZ and OA), since they are responsible for evacuating the control volume when the injector is energized or to refill it when the solenoid stops being energized. The main hydraulic features of these orifices have been identified for several operating conditions, making it possible to explain the fact that the pressure drop in the control volume is higher the lower the fuel temperature, due to the change in the flow regime induced in the OZ orifice through the Reynolds number. The influence of the fuel temperature on the OA orifice performance has been proved to be lower than the one on the OZ orifice, due to the fact that the former always operates in cavitating conditions. Thus, the sole effect of the pressure difference established in the control volume would lead to a faster response of the injector the lower the injection temperature.

- The friction force opposing the needle movement depends on the pressure drop across the needle and the fuel viscosity. Simulations have allowed to conclude that this phenomenon is mostly governed by the fuel viscosity, especially at low temperatures, due to the its exponential increase in those conditions. Thus, the effect of the friction force itself would lead to a slower response of the injector the lower the injection temperature.

- Needle lift laws have been reproduced in order to establish the net effect of the fuel temperature on injection dynamics. Viscous friction has been proved to be the phenomenon dominating the opening stage of the injection, since its variations with temperature have been demonstrated to be larger than those of the pressure drop in the control volume. Thus, the opening stage of the injection is slower the lower the fuel temperature. This, in turn, leads to lower top positions achieved by the needle during its rise due to the ballistic nature of the injector, also resulting in shorter injection durations due to the shorter distance to be travelled by the needle in order to close against its seat.

ACKNOWLEDGEMENTS

This work was partly sponsored by “Ministerio de Economía y Competitividad” in the frame of the project “Comprensión de la influencia de combustibles no convencionales en el proceso de inyección y combustión tipo diesel”, reference TRA2012-36932. The equipment used in this work has been partially supported by FEDER project funds "Dotación de infraestructuras científico técnicas para el Centro Integral de Mejora Energética y Medioambiental de Sistemas de Transporte (CiMeT), (FEDER-ICTS-2012-06)", in the frame of the operation program of unique scientific and technical infrastructure of the Ministry of Science and Innovation of Spain. This support is gratefully acknowledged by the authors.

The authors would also like to thank José Enrique del Rey and Santiago Lacruz for their technical help on the setup of the experimental tools and their support during the measurements.

REFERENCES

[1] Heywood, J.B., Internal combustion engine fundamentals. McGraw-Hill Publishing, 1998, ISBN 007028637X.

[2] Lefèbvre, A.H., Atomization and Sprays, Hemisphere, 1989, ISBN 0891166033.

[3] Hiroyasu, H., Arai, M., Structures of fuel sprays in Diesel engines, SAE Paper 900475, 1990.

[4] Payri, R., Salvador, F.J., Gimeno, J., Ruiz, S., Determination of diesel sprays characteristics in real engine in-cylinder air density and pressure conditions, Journal of Mechanical Science and Technology, 19 (2005), pp. 2040-2052.

[5] Roisman, I.V., Araneo, L, Tropea, C., Effect of ambient pressure on penetration of a diesel spray, International Journal of Multiphase Flow, 33(8) (2007), pp. 904-920.

[6] Agarwal, A.H., Dhar, A., Gupta, J.G., Kim, W.I., et al., Effect of fuel injection pressure and injection timing of Karanja biodiesel blends on fuel spray, engine performance, emissions and combustion characteristics, Energy Conversion and Management, 91 (2015), pp. 302-314.

[7] Zecca, A., Chiari, L., Fossil-fuel constraints on global warming, Energy Policy, 38 (2010), pp. 1-3.

[8] Hall, C.A.S., Lambert, J.G., Balogh, S.B., EROI of different fuels and the implications for society, Energy Policy, 64 (2014), pp. 141-152.

[9] Hessel, R.P., Reitz, R.D., Diesel Engine Injection Rate-Shape Optimization Using Genetic Algorithms and Multi-Dimensional Modeling for a Range of Operating Modes, ILASS –

Europe 2002, 18th Annual Conference on Liquid Atomization & Spray Systems, Zaragoza, 2002.

[10] Salvador, F.J., Hoyas, S., Novella, R., Martínez-López, J., Numerical simulation and extended validation of two-phase compressible flow in diesel injector nozzles, Proceedings of the Institution of Mechanical Engineers, Part D: Journal of Automobile Engineering, 225(4) (2011), pp. 545-563.

[11] Sun, Z.Y., Li, X., Chen, C., Yu, Y., et al., Numerical investigation on effects of nozzle's geometry parameters on the flow and the cavitation characteristics within injector's nozzle for a pressure common-rail DI diesel engine, Energy Conversion and Management, 89(1) (2015), pp. 843-861.

[12] Salvador, F.J., Plazas, A.H., Gimeno, J., Carreres, M., Complete modelling of a piezo actuator last-generation injector for diesel injection systems, International Journal of Engine Research, 15(1) (2014), pp. 3-19.

[13] Payri, R., Salvador, F.J., Martí-Aldaraví, P., Martínez-López, J., Using one-dimensional modeling to analyse the influence of the use of biodiesels on the dynamic behaviour of solenoid-operated injectors in common rail systems: Detailed injection system model, Energy Conversion and Management, 54(1) (2012), pp. 90-99.

[14] Salvador, F.J., Gimeno, J., De la Morena, J., Carreres, M., Using one-dimensional modeling to analyze the influence of the use of biodiesel son the dynamic behavior of solenoid-operated injectors in common rail systems: Results of the simulations and discussion, Energy Conversion and Management, 54(1) (2012), pp. 122-132.

[15] Desantes, J.M., Salvador, F.J., Carreres, M., Jaramillo, D., Experimental Characterization of the Thermodynamic Properties of Diesel Fuels Over a Wide Range of

Pressures and Temperatures, SAE International Journal of Fuels and Lubricants, 8(1) (2015), pp. 190-199.

[16] Dernotte, J., Hespel, C., Houillé, S., Foucher, F., et al., Influence of fuel properties on the diesel injection process in nonvaporizing conditions, Atomization and Sprays, 22(6) (2012), pp. 461-492.

[17] Park, S.H., Kim, H.J., Suh, H.K., Lee, C.S., Experimental and numerical analysis of spray-atomization characteristics of biodiesel fuel in various fuel and ambient temperature conditions, International Journal of Heat and Fluid Flow, 30 (2009), pp. 960-970.

[18] Payri, R., Salvador, F.J., Gimeno, J., Bracho, G., Understanding Diesel Injection Characteristics in Winter Conditions, SAE Technical Paper 2009-01-0836, 2009.

[19] Francisco, J., Jiménez, E., Experimental analysis of low temperature combustion mode with diesel and biodiesel fuels: A method for reducing NOx and soot emissions, Fuel Processing Technology, 103 (2012), pp. 57-63.

[20] Seykens, X.L.J., Somers, L.M.T., Baert, R.S.G., Modelling of common rail fuel injection system and influence of fluid properties on injection process, Proceedings of VAFSEP, Dublin, 2004.

[21] Seykens, X.L.J., Somers, L.M.T., Baert, R.S.G., Detailed modelling of common rail fuel injection process, Journal of Middle European Construction and Design of Cars (MECCA), 3 (2005), pp. 30-39.

[22] Catania, A.E., Ferrari, A., Spessa, E., Temperature variations in the simulation of high-pressure injection-system transient flows under cavitation, International Journal of Heat and Mass Transfer, 51 (2008), pp. 2090-2107.

[23] Mohammed, M.K., Rahman, M.M., Bakar, R.A., Modeling of Common Rail Fuel Injection System of Four Cylinder Hydrogen Fueled Engine, Proceedings of MUCEET2009, Malaysian Technical Universities Conference on Engineering and Technology, Pahang, 2009.

[24] Plamondon, E., Seers, P., Development of a simplified dynamic model for a piezoelectric injector using multiple injection strategies with biodiesel/diesel-fuel blends, Applied Energy, 131 (2014), pp. 411-424.

[25] Rafidah, R., Mamat, R., Taib, M.Y., Abdullah, A.A., Influence of fuel temperature on diesel engine performance operating with biodiesel blend, Journal of Mechanical Engineering and Sciences, 2 (2012), pp. 226-236.

[26] Shi, J., Guerrassi, N., Dober, G., Karimi, K., et al., Complex physics modelling of diesel injector nozzle flow and spray supported by new experiments, Proceedings of THIESEL 2014, 8th International Conference on Thermo- and fluid dynamic processes in direct injection engines, Valencia, 2014.

[27] LMS Imagine.Lab AMESim v.10. User's manual, 2010.

[28] Macián, V., Bermúdez, V., Payri, R., Gimeno, J., New technique for the determination of internal geometry of a diesel nozzle with the use of silicone methodology, Experimental Techniques, 27(2) (2003), pp. 39-43.

[29] Payri, F., Bermúdez, V., Payri, R., Salvador, F.J., The influence of cavitation on the internal flow and the spray characteristics in diesel injection nozzles, Fuel, 83 (2004), pp. 419-431.

[30] Lichtarowicz, A.K., Duggins, R.K., Markland, E., Discharge coefficients for incompressible non-cavitating flow through long orifices, Journal of Mechanical Engineering Science, 7(2) (1965), pp. 210-219.

[31] Soteriou, C., Andrews, R., Smith, M., Direct Injection Diesel Sprays and the Effect of Cavitation and Hydraulic Flip on Atomization, SAE Technical Paper 950080, 1995.

[32] Nurick, W.H., Orifice cavitation and its effect on spray mixing, Journal of Fluids Engineering, 98(4) (1976), pp. 681-687.

[33] Blackburn, J.F., Reethof, G., Shearer, J.L., Fluid Power Control. MIT Press, 1960, ISBN 0262020068.

[34] Adler, U., Bauer, H., Automotive Handbook, Robert Bosch GmbH, Stuttgart, 1995, ISBN 1-56091-918-3.

[35] Desantes, J., Arrègle, J., Rodríguez, P., Computational Model for Simulation of Diesel Injection Systems, SAE Technical Paper 1999-01-0915, 1999.

Table 1: Operating conditions for the experimental mass flow rate measurements used for validation.

Table 2: Summary of nozzle and control orifices geometrical parameters.

Table 3: Summary of the relevant parameters obtained from the hydraulic characterization.

Table 4: Summary of the main parameters of the injector holder.

Table 5: Summary of the main parameters of the magnetic side of the solenoid valve.

Table 6: Summary of the main parameters of the mechanical side of the solenoid valve.

Table 7: Summary of the main parameters of the nozzle.

Table 8: Fuel properties at atmospheric pressure and the temperatures used for model validation.

Table 9: Effect of the fuel injection temperature on the control volume pressure and the friction forces during the opening stage of the injector (time after SOE = 0.7 ms). Reference: T_i = 303 K.

Figure 1: Injector dimensional characterization through the silicone methodology.

Figure 2: Hydraulic characterization experimental setup.

Figure 3: Test rig for the hydraulic characterization of the nozzle.

Figure 4: Nozzle hydraulic characterization results. Left: $\dot{m}$ vs $\sqrt{\Delta P}$; right: C_d vs Re.

Figure 5: Test rig for the hydraulic characterization of the control volume orifices.

Figure 6: OA orifice hydraulic characterization results. Left: $\dot{m}$ vs $\sqrt{\Delta P}$; right: C_d vs Re.

Figure 7: Injector holder detail and model sketch.

Figure 8: Solenoid valve detail of the magnetic path (upper left), mechanical elements (lower left) and model sketch (right).

Figure 9: Nozzle detail and model sketch.

Figure 10: Needle and nozzle optical microscope pictures overlapping.

Figure 11: Mass flow rate model versus experimental results comparison.

Figure 12: Total injected mass: model versus experimental results comparison.

Figure 13: Simplified sketch of the injector during several stages.

Figure 14: Predicted discharge coefficients for the OZ (top) and OA (bottom) orifices according to the flow regime set at the tested operating conditions.

Figure 15: Pressure evolution at the control volume for ET = 1 ms and P_i = 70 MPa (top) and 180 MPa (bottom) at the different fuel temperatures tested.

Figure 16: Force due to viscous friction for ET = 1 ms and P_i = 70 MPa at the different fuel temperatures tested. The force has been normalized with respect to the case at T_i = 303 K.

Figure 17: Needle lift evolution for ET = 1 ms and P_i = 70 MPa (top) and 180 MPa (bottom) at the

different fuel temperatures tested.

Figure 18: Normalized maximum needle lift reached for all the tested injector operating conditions.

T_i [K]	P_i [MPa]	ET [ms]	P_b [MPa]
253 273 303 353 373	40 70 120 180	0.25 0.5 1 2	4

Table 1: Operating conditions for the experimental mass flow rate measurements used for validation.

Orifice	D_i [µm]	D_o [µm]	*k-factor* [µm]
Nozzle (7 orifices)	146±2	117±1	2.8±0.2
OZ	308	290	1.8
OA	256	259	-0.3

Table 2: Summary of nozzle and control orifices geometrical parameters.

Orifice	C_{dmax}	Re_{crit}	CN_{crit}	C_c
Nozzle (7 orifices)	0.96	5600	-	-
OZ	0.94	7000	-	-
OA	0.95	7200	1.24	0.71

Table 3: Summary of the relevant parameters obtained from the hydraulic characterization.

Element	Length [mm]	Diameter [mm]	Volume [mm^3]	Mass [g]
Rail	-	-	24000	-
Filter	-	0.8	-	-
HL1	7.38	1.38	-	-
HV1	-	-	13.5	-
HL2	8.75	1.1	-	-
HV2	-	-	1.85	-
HL3	17.05	1	-	-
HL4	40.64	1.5	-	-
HL5	49.9	1.5	-	-
HV3	-	-	81	-
HV4	-	-	25	-
1/2 NM	-	-	-	4.6
Element	Piston diameter [mm]		Rod diameter [mm]	Spring rate [N/m]
P1	4.3		0	-
LF	4.3		4.292	-
P2	4.3		4	-
ND	-		-	$8.5 \cdot 10^7$
NSP	-		-	5250

Table 4: Summary of the main parameters of the injector holder.

Element	Length [mm]	Area [mm^2]
SM1	6.725	136.07
SM2	3	108.38
SM3	6.725	51.25
SM4	3	108.38
AG	0.08	31.82

Element	No. coils [-]	Resistance [Ω]
Coil	40	7.46

Table 5: Summary of the main parameters of the magnetic side of the solenoid valve.

Element	Length [mm]	Diameter [mm]	Volume [mm^3]	Mass [g]
SO2	-	1.255	-	-
SO3	-	5.233	-	-
SO4	-	1.0	-	-
SL1	8.25	5.0	-	-
SL2	23.25	5.0	-	-
SV1	-	-	23	-
SV2	-	-	522.2	-
SV3	-	-	5.3	-
VM	-	-	-	3.1
Element	Piston diameter [mm]		Rod diameter [mm]	Spring rate [N/m]
SP1	3.6		1.6	-
SP2	4.3		3.6	-
SP3	12.5		4.3	-
SP4	12.5		1.5	-
SLF	4.5		4.3	-
SS	-		-	38070

Table 6: Summary of the main parameters of the mechanical side of the solenoid valve.

Element	Length [mm]	Diameter [mm]	Volume [mm^3]
NL1	3.5	0.7	-
NO1	-	0.37	-
NL2	20.75	0.7	-
NV1	-	-	2.68
NL3	5	0.5	-
NV2	-	-	6.36
NV3	-	-	0.3
NST	-	0.6	-
Element	Piston diameter [mm]	Rod diameter [mm]	Mass [g]
NP1	4	3.16	-
NP2	3.16	1.81	-
1/2 NM	-	-	4.6

Table 7: Summary of the main parameters of the nozzle.

Fuel temperature [K]	Density [kg/m^3]	Absolute viscosity [cP]
253	851	15.32
273	838	5.87
303	820	2.71
353	785	1.1
373	775	0.85

Table 8: Fuel properties at atmospheric pressure and the temperatures used for model validation.

T_i [K]	$\frac{P_{cv}}{P_{cv\_303K}}$		$\frac{F_{fric}}{F_{fric\_303K}}$	
253	0.852	↓	2.224	↑↑↑
273	0.952	↓	1.757	↑↑
303	1		1	
353	1.002	≈	0.415	↓↓
373	1.005	≈	0.346	↓↓↓

Table 9: Effect of the fuel injection temperature on the control volume pressure and the friction forces during the opening stage of the injector (time after SOE = 0.7 ms). Reference: T_i = 303 K.

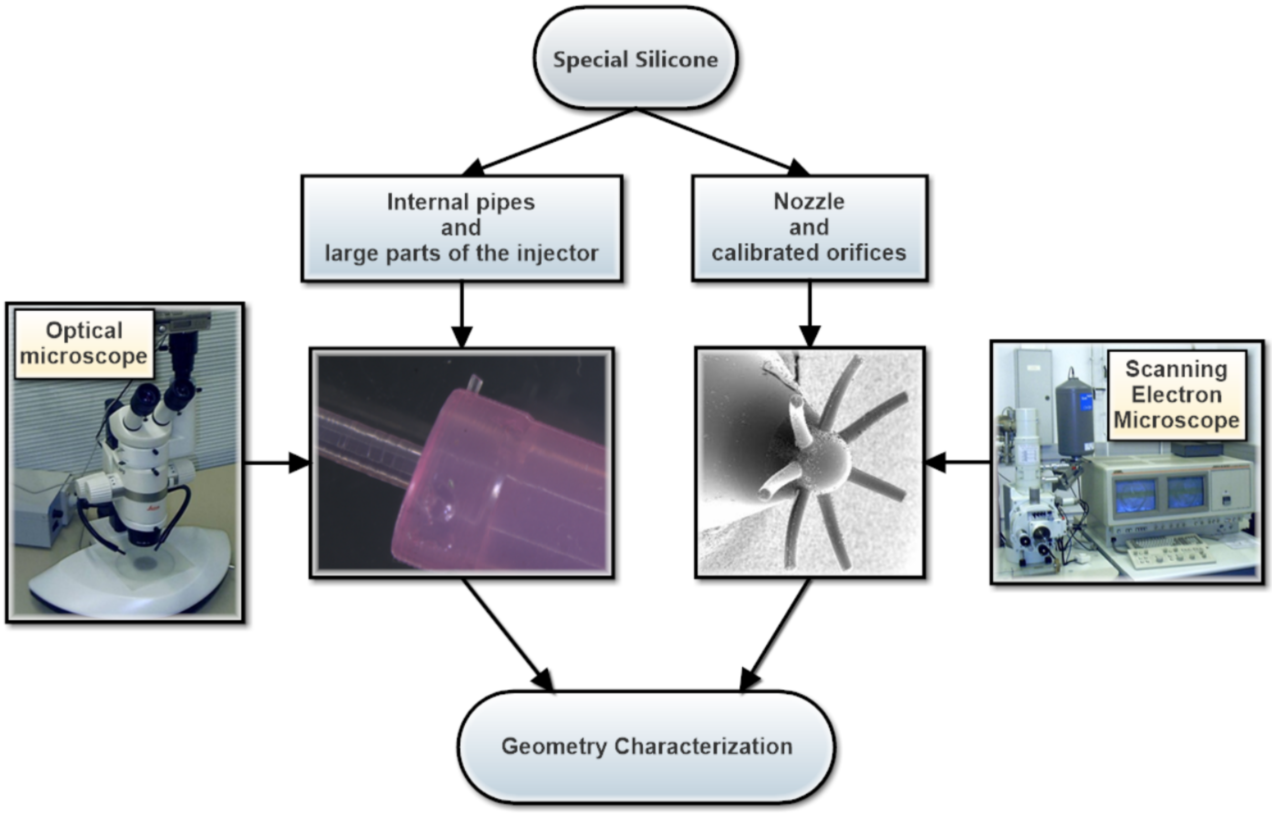

Figure 1: Injector dimensional characterization through the silicone methodology.

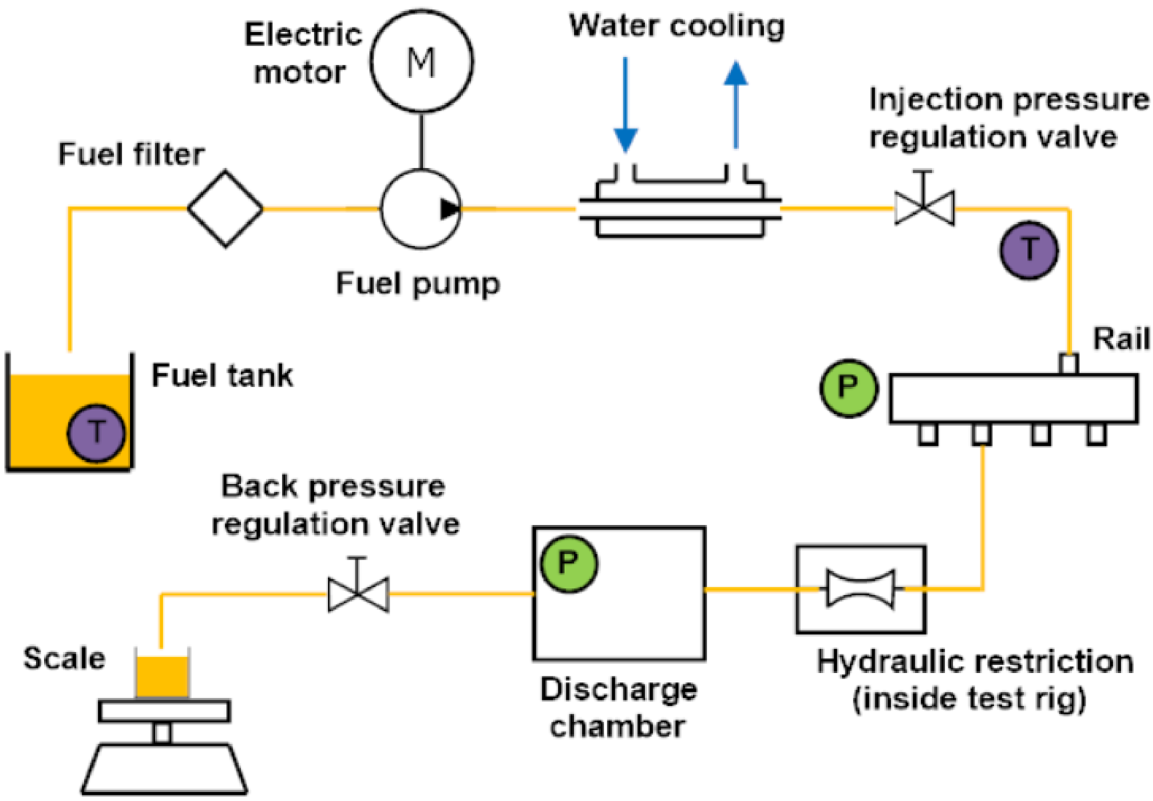

Figure 2: Hydraulic characterization experimental setup.

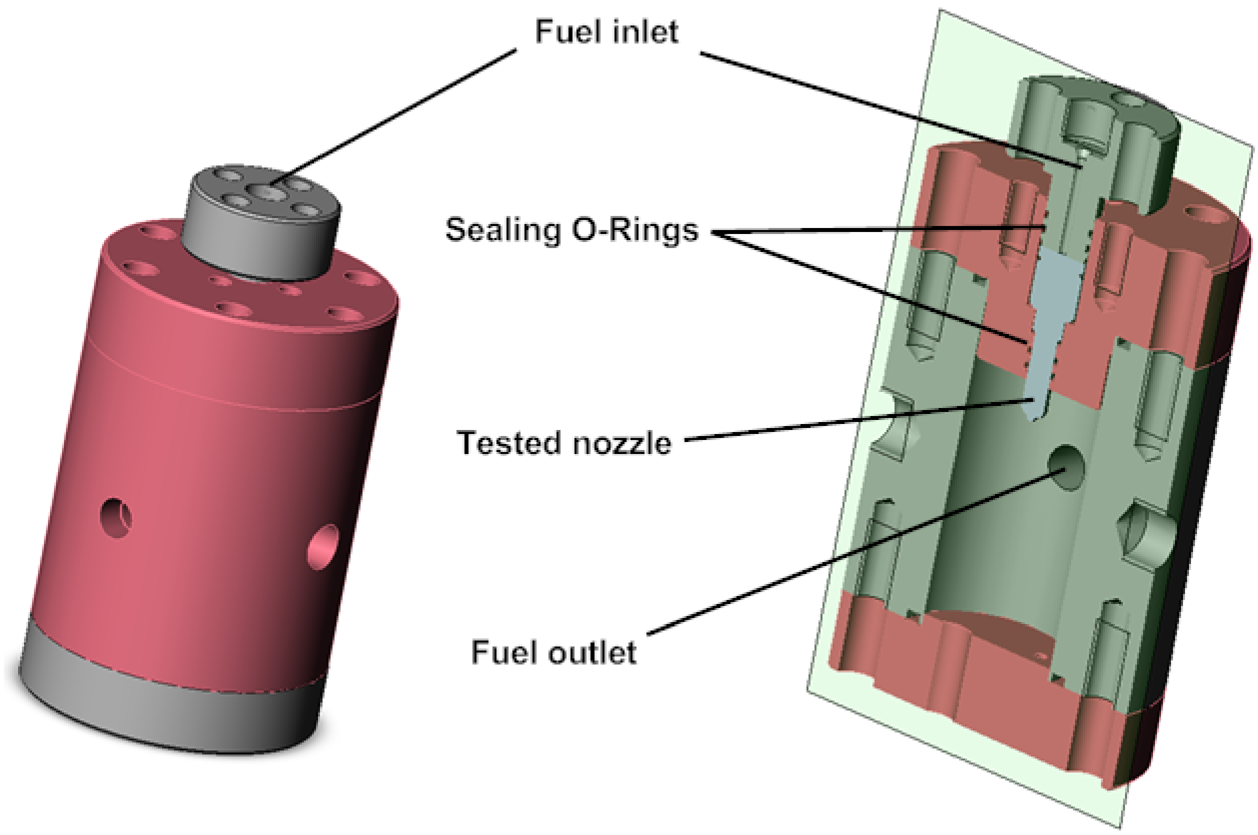

Figure 3: Test rig for the hydraulic characterization of the nozzle.

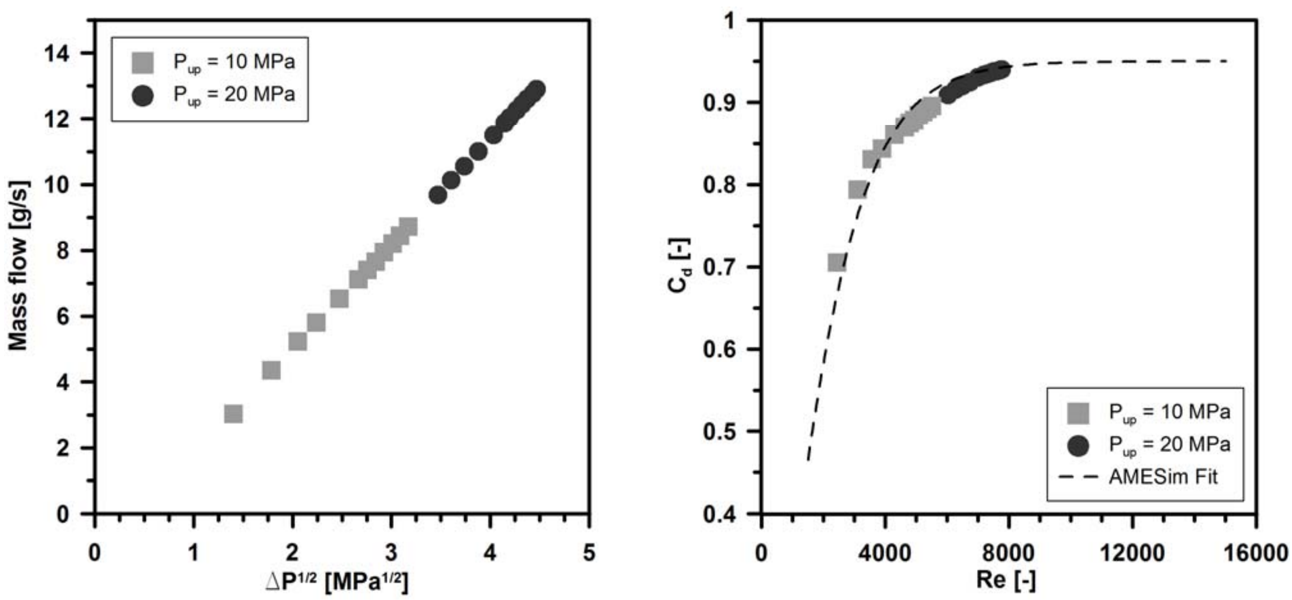

Figure 4: Nozzle hydraulic characterization results. Left: $\dot{m}$ vs $\sqrt{\Delta P}$; right: C_d vs Re.

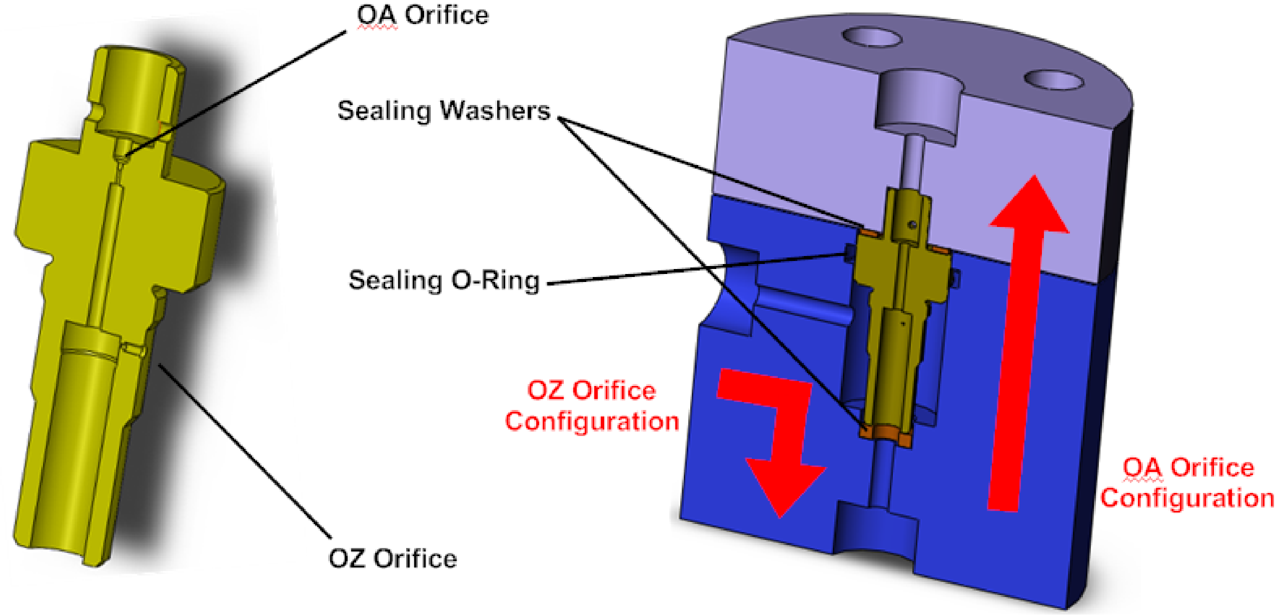

Figure 5: Test rig for the hydraulic characterization of the control volume orifices.

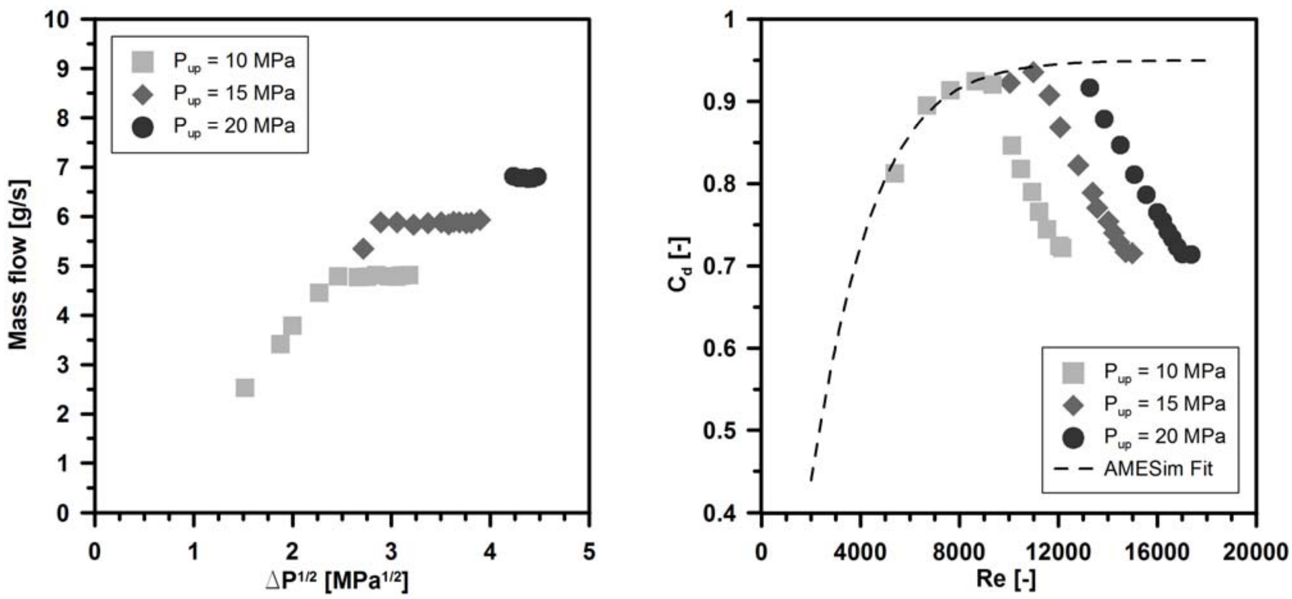

Figure 6: OA orifice hydraulic characterization results. Left: $\dot{m}$ vs $\sqrt{\Delta P}$; right: C_d vs Re.

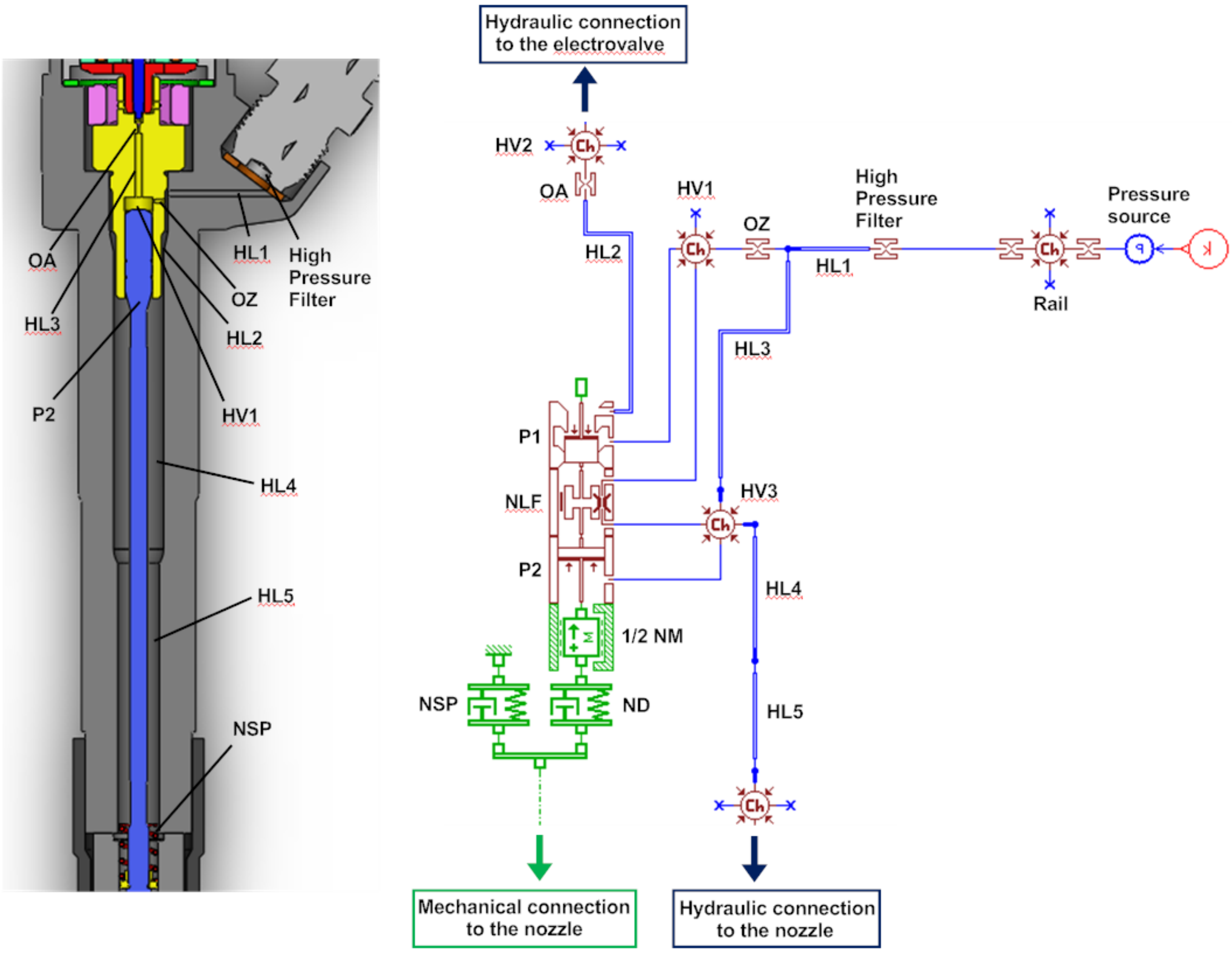

Figure 7: Injector holder detail and model sketch.

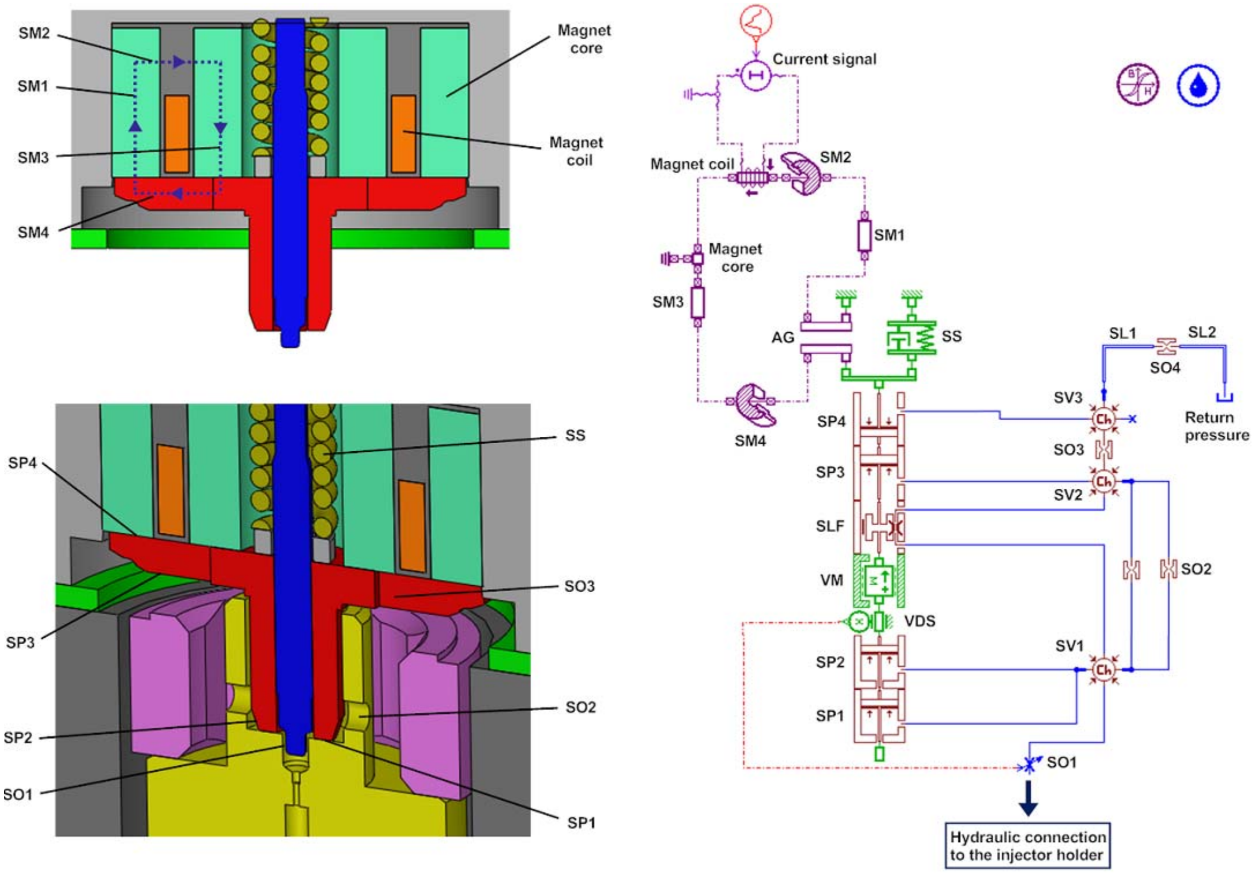

Figure 8: Solenoid valve detail of the magnetic path (upper left), mechanical elements (lower left) and model sketch (right).

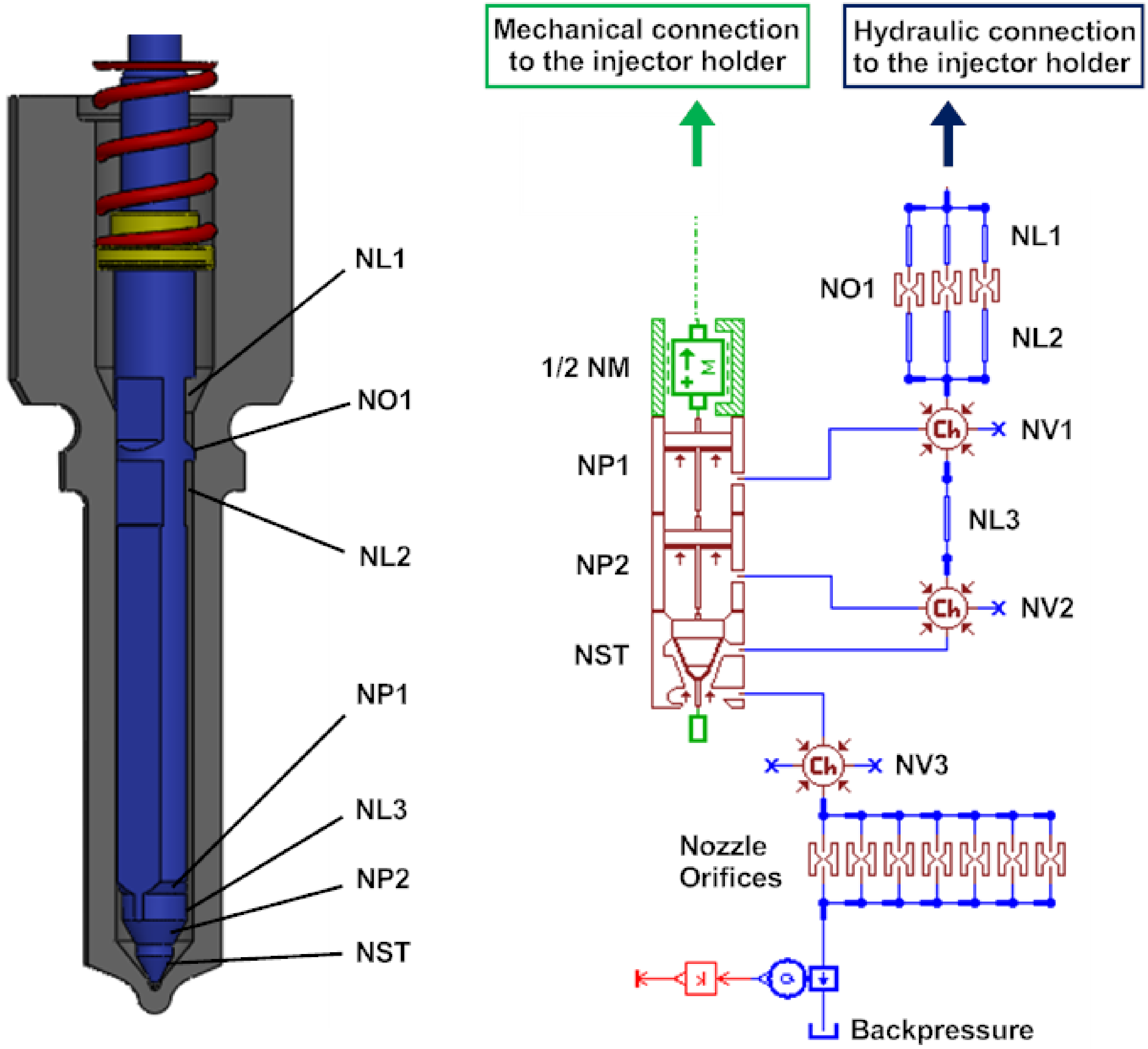

Figure 9: Nozzle detail and model sketch.

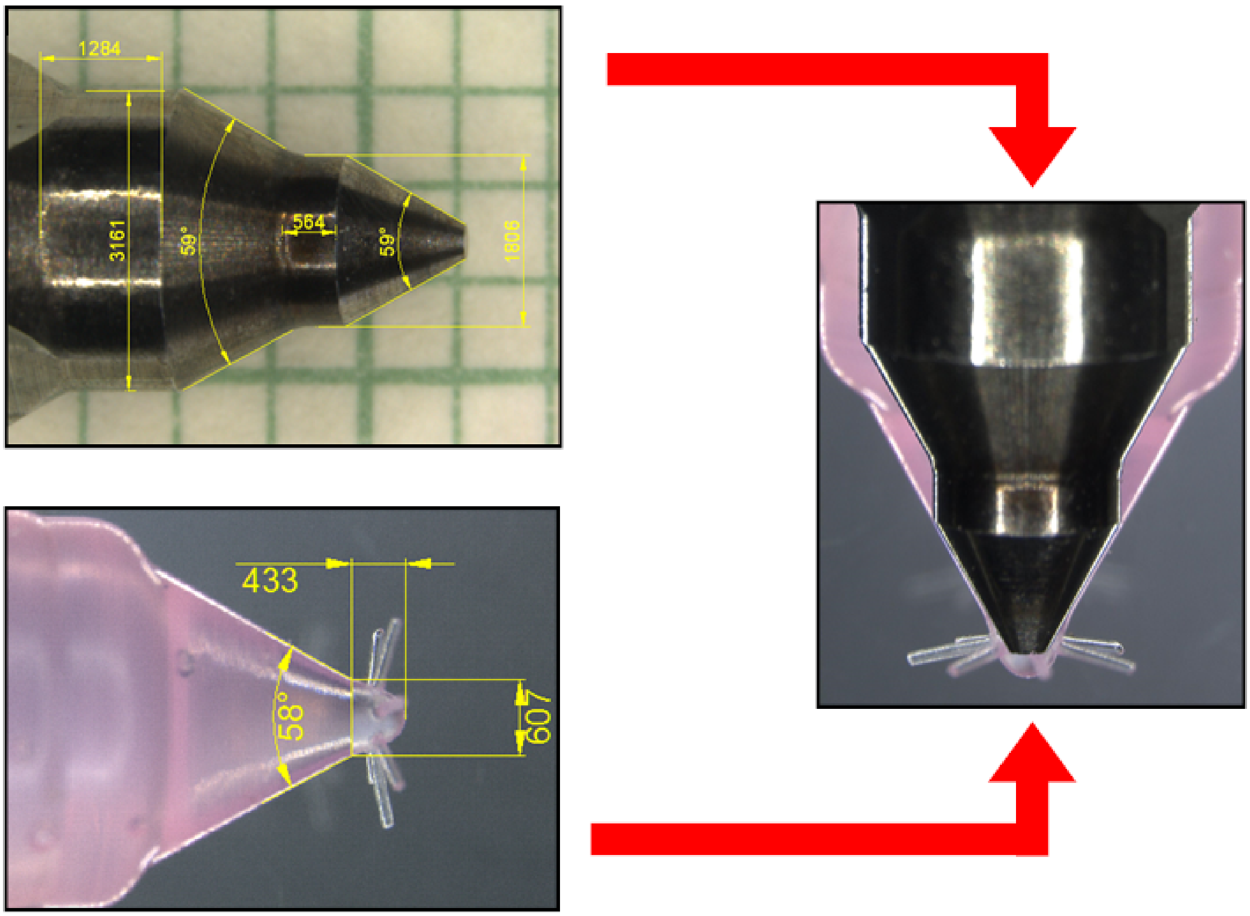

Figure 10: Needle and nozzle optical microscope pictures overlapping.

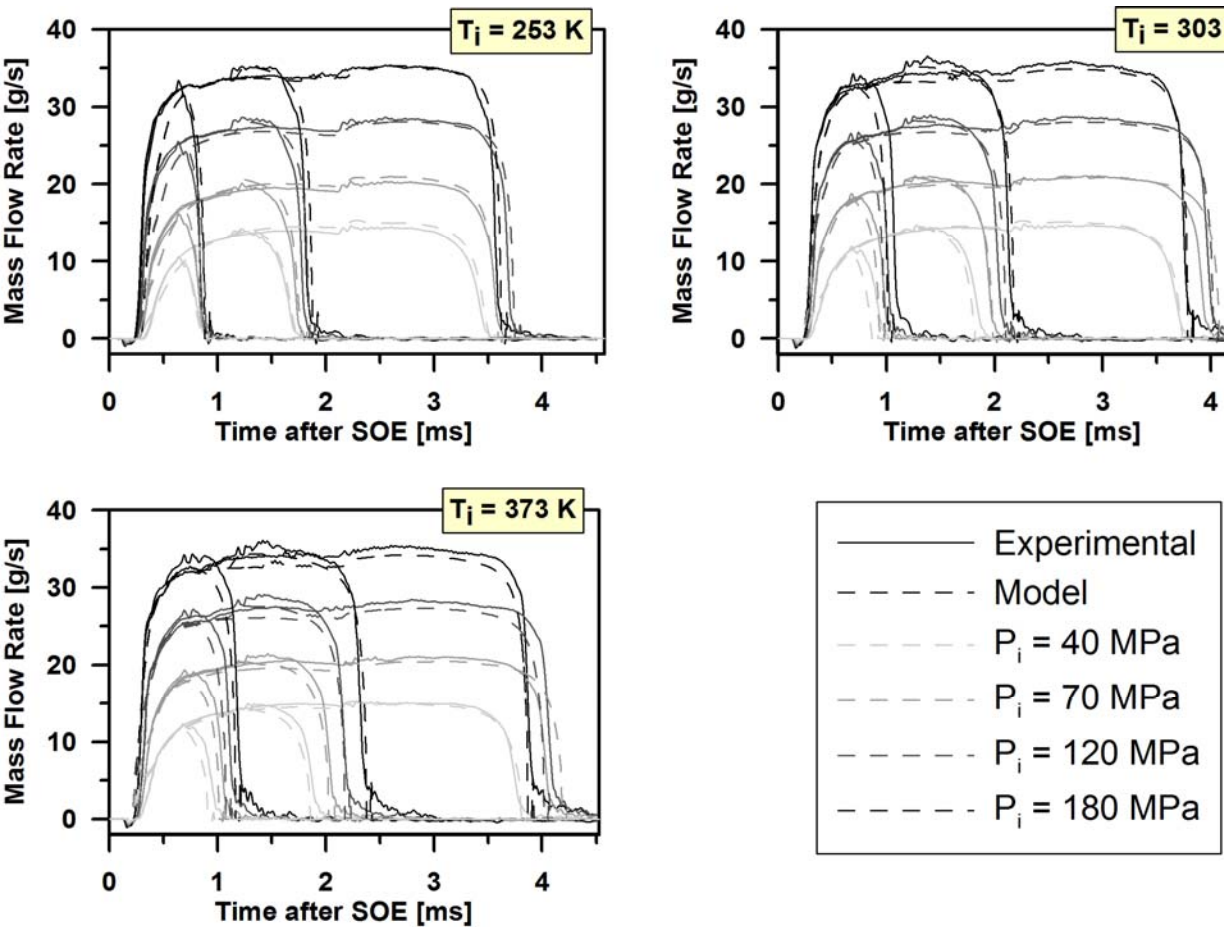

Figure 11: Mass flow rate model versus experimental results comparison.

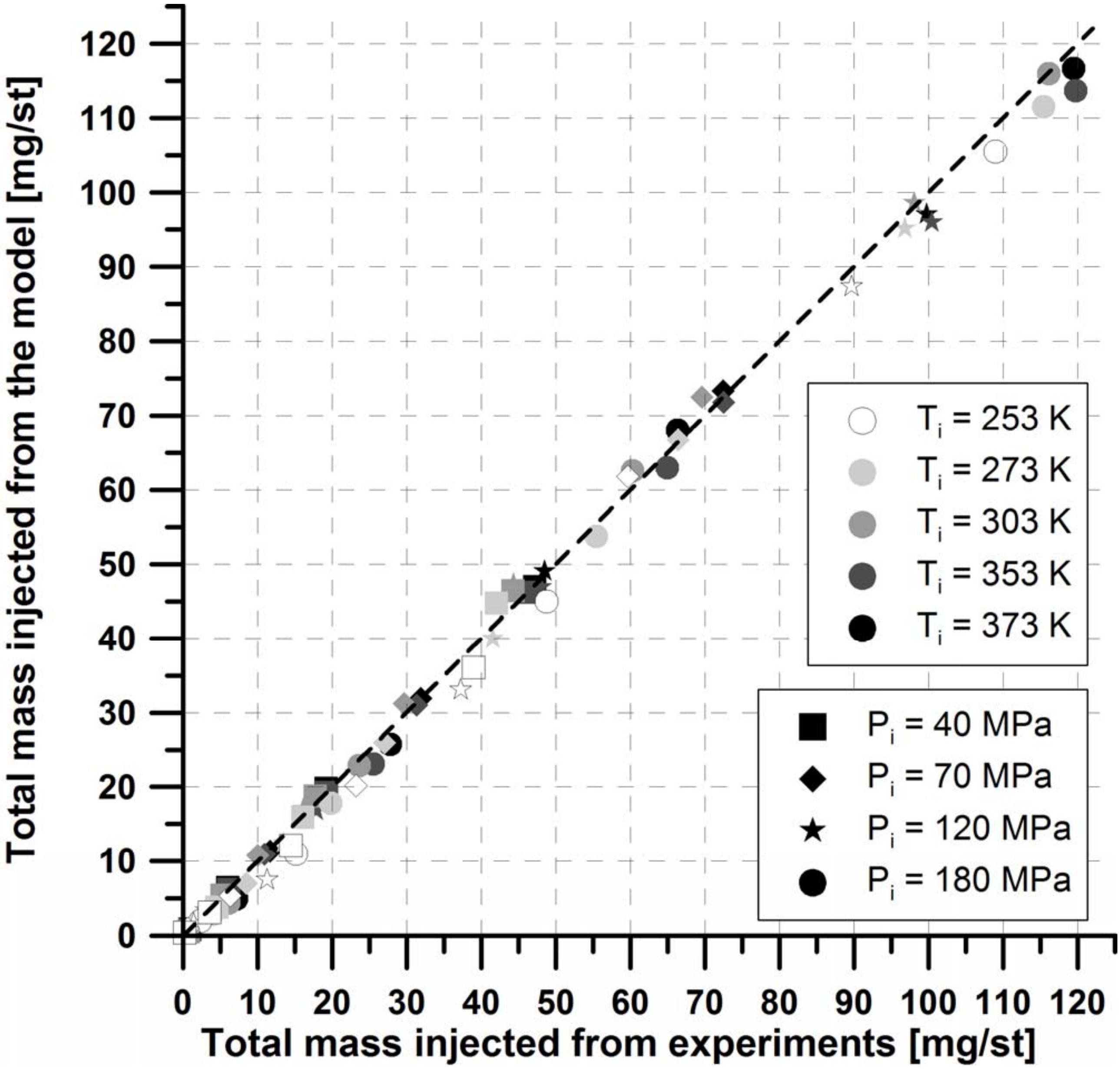

Figure 12: Total injected mass: model versus experimental results comparison.

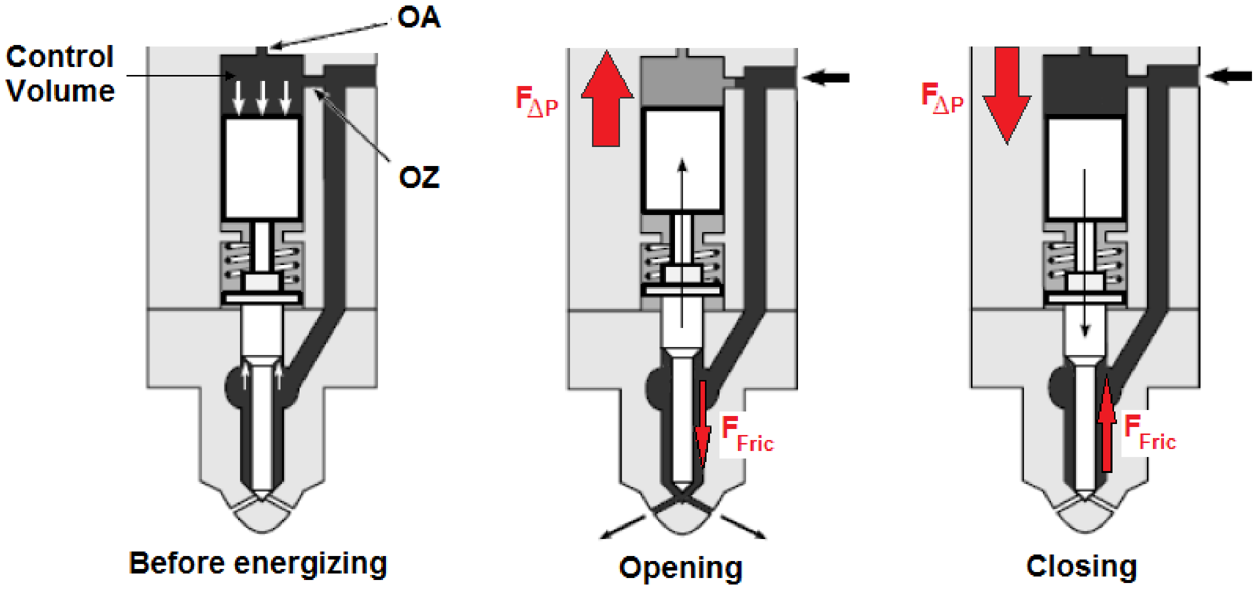

Figure 13: Simplified sketch of the injector during several stages.

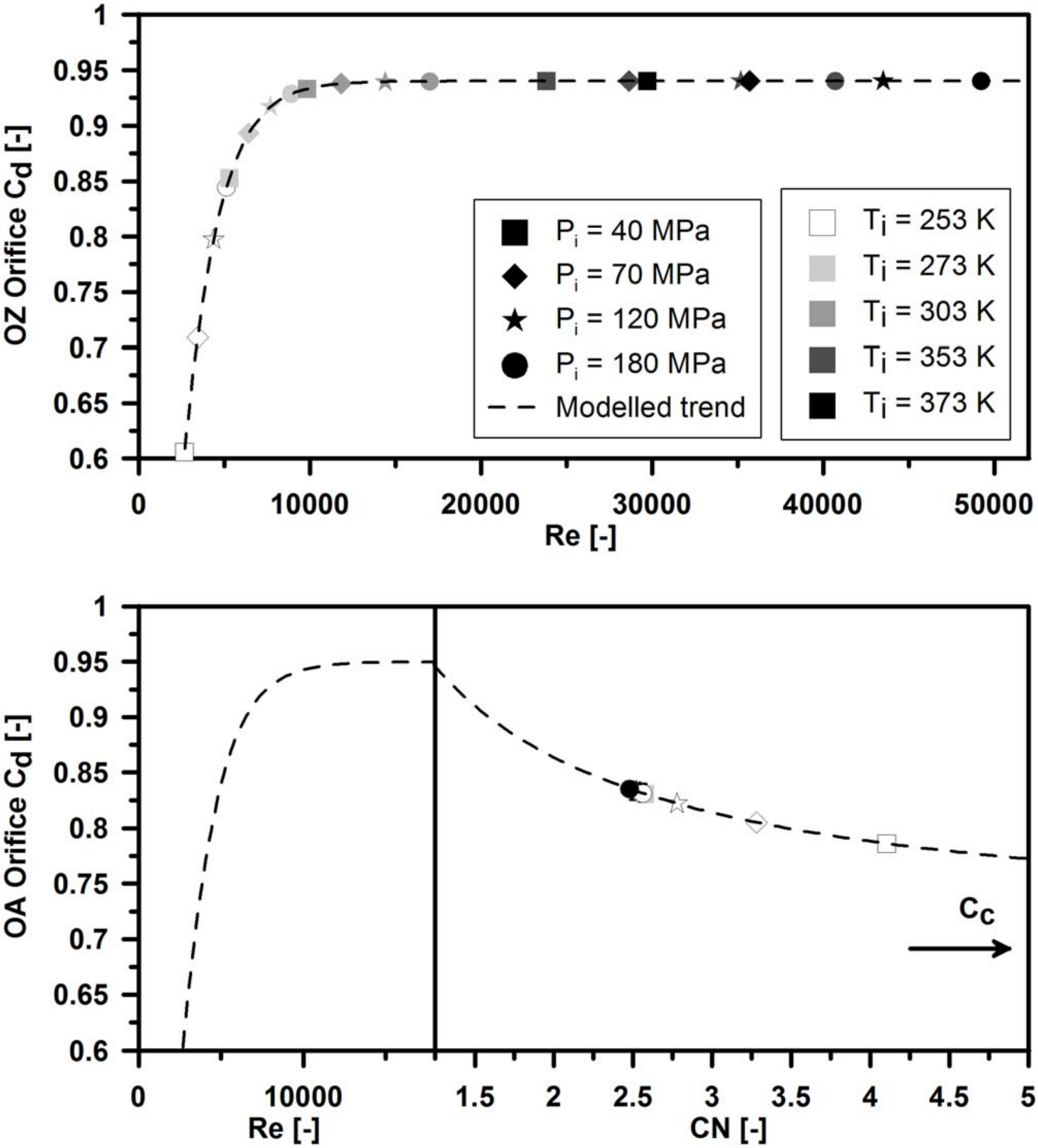

Figure 14: Predicted discharge coefficients for the OZ (top) and OA (bottom) orifices according to the flow regime set at the tested operating conditions.

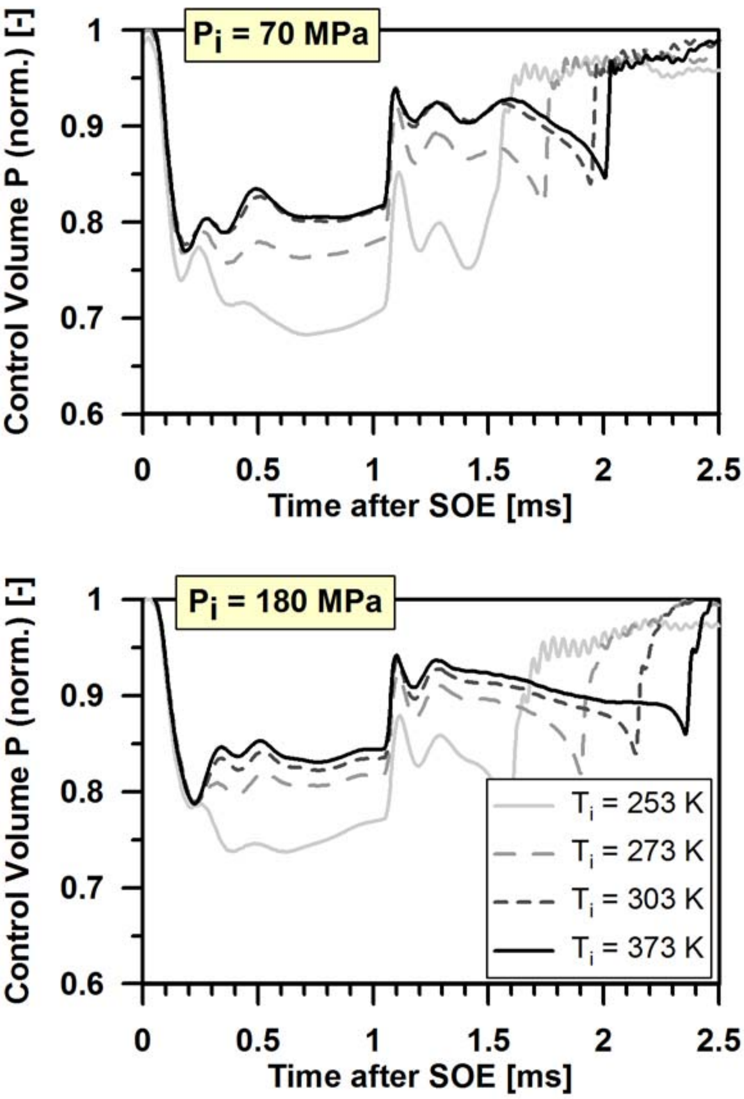

Figure 15: Pressure evolution at the control volume for *ET* = 1 ms and P_i = 70 MPa (top) and 180 MPa (bottom) at the different fuel temperatures tested.

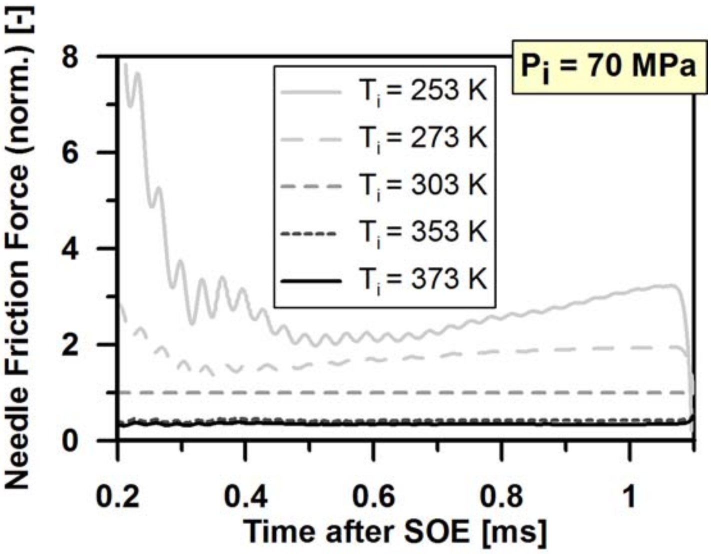

Figure 16: Force due to viscous friction for ET = 1 ms and P_i = 70 MPa at the different fuel temperatures tested. The force has been normalized with respect to the case at T_i = 303 K.

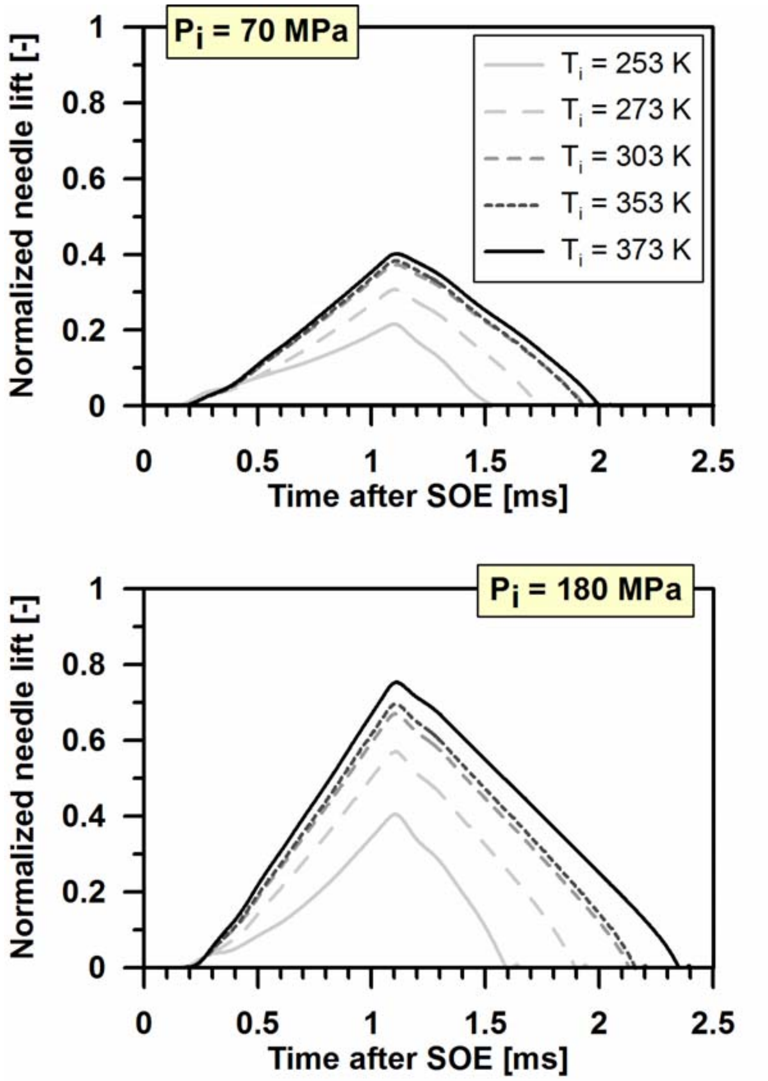

Figure 17: Needle lift evolution for $ET = 1$ ms and $P_i = 70$ MPa (top) and 180 MPa (bottom) at the different fuel temperatures tested.

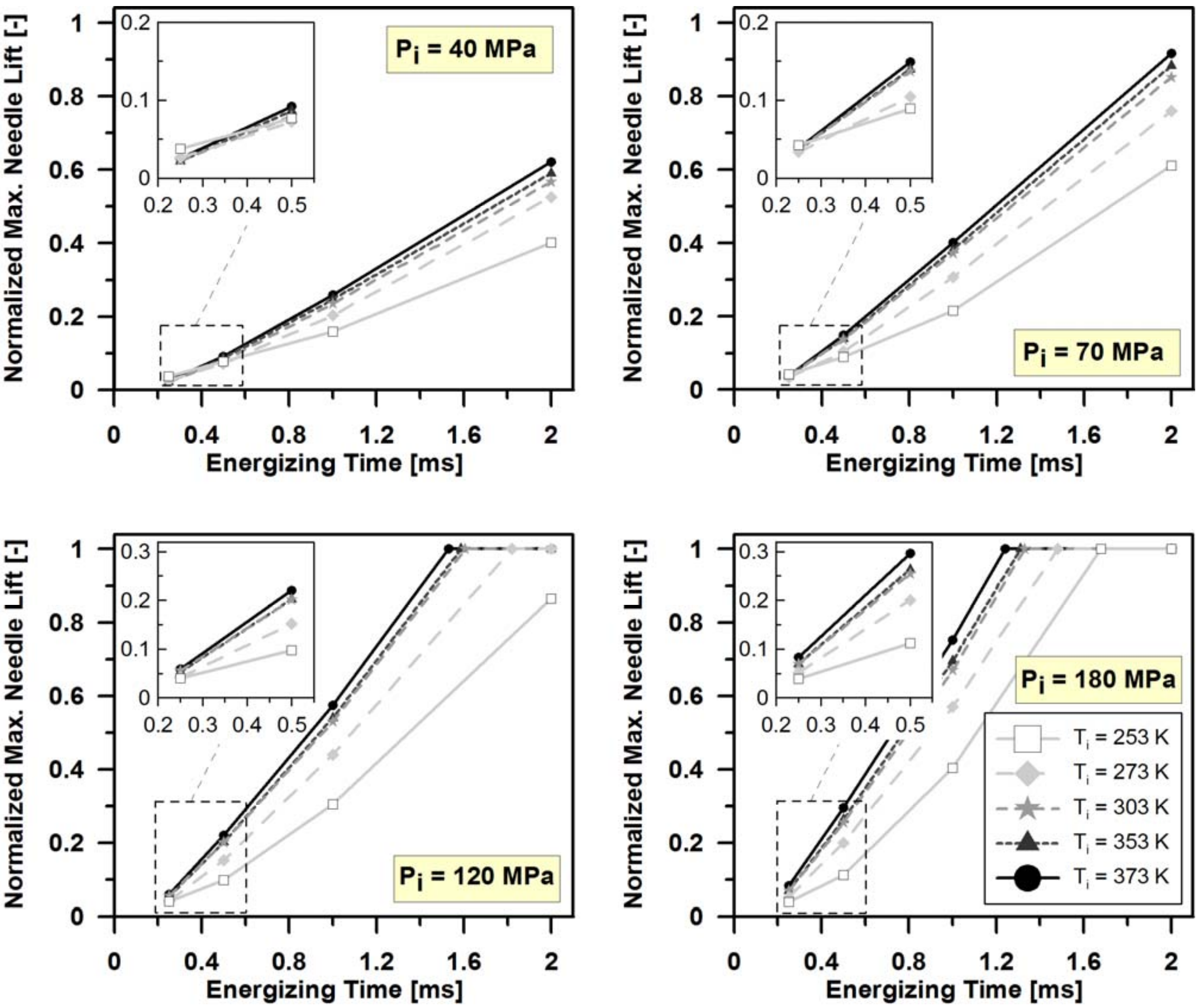

Figure 18: Normalized maximum needle lift reached for all the tested injector operating conditions.